Earth-Science Reviews 203 (2020) 103111

Contents lists available at ScienceDirect

Earth-Science Reviews

journal homepage: www.elsevier.com/locate/earscirev

Invited review

Mercury stable isotopes for monitoring the effectiveness of the Minamata Convention on Mercury

Sae Yun Kwon[a,*], Joel D. Blum[b], Runsheng Yin[c], Martin Tsz-Ki Tsui[d], Yo Han Yang[a], Jong Woo Choi[e]

[a] Division of Environmental Science and Engineering, Pohang University of Science and Technology, 77 Cheongam-Ro, Nam Gu, Pohang 37673, South Korea
[b] Department of Earth and Environmental Sciences, University of Michigan, 1100 N. University Ave, Ann Arbor, Michigan 48109, United States of America
[c] State Key Laboratory of Ore Deposit Geochemistry, Institute of Geochemistry, Chinese Academy of Sciences, 55081 Guiyang, China
[d] Department of Biology, University of North Carolina at Greensboro, 321 McIver Street, Greensboro, NC 27402, United States of America
[e] Environmental Measurement and Analysis Center, National Institute of Environmental Research, 42 Hwangyong-Ro, Seo-Gu, Incheon 22689, South Korea

ARTICLE INFO

Keywords:
Mercury
Stable isotope
Minamata Convention
Monitoring
Effectiveness evaluation
Policy

ABSTRACT

The Minamata Convention on Mercury (MC) includes provisions for a global monitoring program (GMP) and effectiveness evaluation (EE) to provide information on changes in mercury sources in various environmental media. While conventional measurement and modeling techniques have limitations in explaining the changes in mercury concentrations, the measurements of natural abundances of mercury stable isotopes have become powerful tracers for distinguishing between mercury sources and for understanding biogeochemical processes in the environment. Unfortunately, it is uncertain whether mercury isotope ratios can provide globally comparable results on specific mercury sources for the GMP and trend analyses for the EE. We have compiled a dataset from the literature to evaluate large-scale patterns of mercury isotope ratios in various environmental samples and to summarize sample types that can be used for the GMP. Total gaseous mercury, precipitation, foliage, and litter can provide comparable source information regarding atmospheric mercury across a large spatial scale. Interpretation of spatially relevant information using sediment and fish mercury isotope ratios are challenging because they represent multiple mercury sources and contain mercury that has been subject to biogeochemical transformation leading to isotope fractionation. In regards to the EE, data that provides evidence of changes due to source regulation needs to be gathered from local point source regions to assess health impacts. We recommend that the measurements of particulate-bound mercury in the atmosphere and sediment mercury isotope ratios near mercury hotspots and in fish, are needed to identify ecosystems sensitive to atmospheric deposition and to evaluate the effectiveness of the MC.

1. Introduction

Mercury is registered as one of the top ten chemicals of public health concern by the World Health Organization (WHO, 2018). Mercury travels long distances in the atmosphere as gaseous elemental mercury (Hg^0) and deposits to aquatic and terrestrial ecosystems as oxidized (Hg^{2+}) and particulate-bound mercury species (Hg_P) via dry and wet deposition (Selin, 2009). Mercury is subject to microbial methylation and the production of highly toxic monomethylmercury (MMHg) in the water column, surface sediments, and wetlands, which then can biomagnify through food webs. Humans are primarily exposed to MMHg via fisheries product consumption (Mergler et al., 2007).

After decades of research, development, and multi-stakeholder efforts, the Minamata Convention on Mercury (MC), a multilateral agreement to mitigate human health impacts from mercury pollution, entered into force in August 2017 (UN Environment, 2017a). Anthropogenic activities including fossil fuel combustion, metal smelting, waste incineration, and cement production are expected to be regulated through implementation of mercury capture technologies and policies, which enforce upstream reductions in mercury emissions and releases (Article 8, 9). Direct mercury mining as well as mercury supply and trade (Article 3) for artisanal and small-scale gold mining (ASGM; Article 7), consumer products (Article 4), and manufacturing (Article 5) are subject to phase-outs by the year 2020. As a part of the MC, provisions have also been established for a global monitoring program (GMP) and a convention effectiveness evaluation (EE; Article 19, 22) with the goal of understanding the presence and changes in mercury levels, compounds, and sources (natural, anthropogenic, legacy) as well

* Corresponding author.
E-mail address: saeyunk@postech.ac.kr (S.Y. Kwon).

https://doi.org/10.1016/j.earscirev.2020.103111
Received 18 August 2019; Received in revised form 28 January 2020; Accepted 29 January 2020
Available online 30 January 2020

as their movement, transformation, and fate in various environmental media, including biota (UN Environment, 2017a). While the precise scope and the distinction between the GMP and EE are still being discussed within the technical experts group (an international group of academics, government officials, and policy officers that are experts in specific areas of the MC and report to the intergovernmental negotiating committee on mercury), these objectives share common opportunities and challenges. The major opportunities are that they promote multilateral capacity building through existing and new mercury monitoring operations and stimulate scientific advancements to better measure and model mercury in the environment (Gustin et al., 2016). The major challenges are establishing an internationally comparable performance indicator that can distinguish between changes in mercury sources subject to regulation and differentiate other influences on mercury from the environment such as climate change (i.e., changes in precipitation patterns; Mao et al., 2017; Perlinger et al., 2018; Sprovieri et al., 2017; surface temperature; Chen et al., 2015; biomass burning; Friedli et al., 2009; Kumar et al., 2018) and other human activities (i.e., urbanization, land-use change; Domagalski et al., 2016; Drevnick et al., 2016; Fleck et al., 2016), which may interfere with the identification of MC-relevant changes in mercury sources. Identifying appropriate environmental media and the form of mercury used to monitor changes in sources, movement, transformation, and fate also requires a spatiotemporal level of understanding regarding atmospheric and biogeochemical cycling of mercury.

The common challenges shared by the GMP and the EE have become increasingly evident through long-term measurement and modeling studies. Slemr et al. (2011) observed a 20-38% reduction in atmospheric Hg^0 concentrations in the Northern and Southern Hemisphere between 1995 and 2010 and attributed this to climate change-related reduction in soil and ocean surface re-emissions. Using a global scale atmospheric chemistry transport model (GEOS-Chem) coupled to 2-D land and ocean reservoirs, Soerensen et al. (2012) and Zhang et al. (2016) provided contrasting explanations for the observed reduction–either changes in atmospheric mercury oxidation, riverine mercury input to the oceans, or a widespread phase-out of mercury-containing products. In regards to ecosystem fate of atmospheric mercury, Perlinger et al. (2018) used the same model (GEOS-Chem) to simulate future atmospheric mercury deposition to the Great Lakes region and estimated that there could be between a 78% reduction and a 5.2% increase in atmospheric mercury deposition under a strict MC scenario or a climate change-related increase in precipitation, respectively. By coupling future atmospheric mercury deposition with a lake mass balance model, the same study found that fish mercury concentration is more sensitive to local landscape and land use characteristics (e.g., the presence and abundance of wetlands) compared to the widespread upstream regulation of anthropogenic mercury emissions via the MC (Perlinger et al., 2018). Recent synthesis studies compiling large datasets have also shown that environmental factors influencing MMHg production may be more important in explaining observed sediment and fish MMHg concentrations across western U.S. freshwater bodies compared to direct inorganic mercury (IHg; Hg^0 + Hg^{2+} + Hg_P) loading via wet deposition (Eagles-Smith et al., 2016a, 2016b; Fleck et al., 2016). The ability to identify mercury sources subject to regulation and factors affecting mercury source-fate relationships will become important as the international effort to regulate mercury progresses.

The measurements of natural abundances of mercury stable isotopes in environmental samples can serve as a valuable tool for addressing the challenges of the GMP and EE. Until recently, mercury isotope studies were conducted primarily on local to regional scales and in conjunction with concentration and speciation analyses to characterize different types of anthropogenic (i.e., coal-fired power plant, smelting, mercury and gold mining, chemical industries) and natural (i.e., terrestrial runoff, biomass burning, volcanic emission) mercury sources and to understand the movement, transformation, and fate of mercury in the atmosphere and in aquatic and terrestrial environments (e.g., Blum et al., 2014). Development of new methodological approaches to establish linkages between environmental sources of mercury and biota (Kwon et al., 2014; Tsui et al., 2012) and timescale assessments for biological and ecological mercury transfers (i.e., internal distribution, tissue turnover, bioaccumulation, trophic transfer; Kwon et al., 2012, 2013, 2016) have provided insight into how biota may respond to changes in mercury sources. Mercury isotope ratios of biota are also increasingly being used to gather site-specific information governing mercury source-fate relationships. For instance, previous studies have observed south to north declines in $\Delta^{199}Hg$ and $\Delta^{200}Hg$ in seabird eggs and mammalian liver tissues, consistent with the latitudinal increase in sea ice cover across the Arctic Ocean (Day et al., 2012; Masbou et al., 2018). The authors suggested that in the high Arctic, where sea ice cover modifies atmospheric deposition and photoreduction of mercury in the water column, terrestrial mercury sources may be an important mercury source to marine biota. Such insight can be considered as an ecosystem or environmental baseline, which provides critical information for understanding the present and for predicting ecosystem responses to future upstream regulations of mercury under the MC.

In 2016, a year prior to the first MC's Conference of the Parties (COP1), the potential utility of mercury isotopes for the GMP and EE was entered into the discussion among mercury monitoring and modeling communities (e.g., Gustin et al., 2016; Kwon and Selin, 2016). However, uncertainties and limitations still remain in the application of mercury isotopes for the GMP and EE. The uncertainties arise from the MC's objective of generating "comparable results [on mercury sources, movement, transformation, and fate] on a global basis" for the GMP. To this date, mercury isotope measurements have not been evaluated on a large enough spatiotemporal scale to assess whether the differences in mercury sources and processes could be deciphered on a global scale. The limitation arises from the lack of distinction in the assigned activity and scope between the GMP and EE. The expert group currently aims to identify "how monitoring activities [from the GMP] may contribute to the development of the effectiveness evaluation framework" including the assessment of "trends in levels of mercury and mercury compounds". This means that the EE may simply reflect trend analyses from the GMP data.

The purpose of this review paper is 1) to evaluate large scale patterns of mercury isotope ratios in various environmental samples and ecosystems for the GMP, and 2) to illustrate why the measurement of mercury isotopes on a local scale may be important for addressing the challenges of the EE. Following the Introduction (Section 1), the review is organized as follows:

- Section 2 introduces mercury isotope systematics including the reporting nomenclature, mixing relationships, and different types of fractionation pathways.
- Section 3 evaluates large scale patterns of mercury isotope ratios in various environmental samples and ecosystems (samples from the atmosphere, terrestrial, and aquatic environments), which are generated from a compilation of previously reported mercury isotope ratios from the literature (Table A.1).
- Section 4 summarizes specific environmental sample types that may be used to establish isotopically comparable results on mercury sources, processes, and fate on a large spatial scale for the GMP.
- Section 5 proposes a new scope for the EE that is aligned with the MC's purpose of mitigating ecosystem and human health impacts from mercury exposure and illustrates why mercury isotope measurements on a local scale may be important for the EE.

2. Mercury stable isotope systematics

Mercury stable isotopes exist naturally in the environment and have the following approximate abundances ($^{196}Hg = 0.155\%$, $^{198}Hg = 10.04\%$, $^{199}Hg = 16.94\%$, $^{200}Hg = 23.14\%$, $^{201}Hg = 13.17\%$,

^{202}Hg = 29.73%, ^{204}Hg = 6.83%; Blum and Bergquist, 2007). They undergo mixing and fractionation during biogeochemical reactions, which slightly modifies the isotope ratios of mercury in environmental samples (e.g., Blum et al., 2014). Precise measurements of mercury isotope ratios were made possible beginning in the 2000s using multi-collector inductively coupled plasma mass spectrometry (MC-ICP-MS). The development of protocols to measure and report mercury isotope ratios (Blum and Bergquist, 2007) have also enabled consistent data comparison among international research groups.

2.1. Mass-dependent fractionation

Mercury isotopes undergo three overall types of stable isotope fractionation pathways—mass-dependent fractionation, mass-independent fractionation of odd mass number isotopes and mass-independent fractionation of even mass number isotopes. Mass-dependent fractionation (MDF) is reported as δ^{202}Hg in permil (‰) referenced to the commonly adopted isotope reference material for mercury, NIST 3133;

$$\delta^{202}\mathrm{Hg} = [(^{202}\mathrm{Hg}/^{198}\mathrm{Hg})_{\mathrm{sample}}/(^{202}\mathrm{Hg}/^{198}\mathrm{Hg})_{\mathrm{NIST3133}} - 1] \times 1000 \quad (1)$$

The pattern of MDF is similar to the traditional light isotope systems (i.e., carbon and nitrogen) such that the degree of fractionation is proportional to the mass differences between the isotopes. Thus far, many kinetic processes have been shown to cause measurable MDF, particularly in the aqueous phase, including photoreduction of inorganic mercury (IHg), photodegradation of MMHg (Bergquist and Blum, 2007; Chandan et al., 2014; Zheng and Hintelmann, 2009, 2010a), dark reduction of Hg^{2+} (Zheng and Hintelmann, 2010b), microbial methylation and demethylation (Janssen et al., 2016; Kritee et al., 2009; Perrot et al., 2015; Rodriguez-Gonzalez et al., 2009), abiotic methylation (Jiménez-Moreno et al., 2013), and diffusion (Koster van Groos et al., 2013) and volatilization of Hg^0 (Zheng et al., 2007). Equilibrium reactions including dark oxidation of Hg^0 (Zheng et al., 2019), mineral sorption (Jiskra et al., 2012), thiol-ligand exchange (Wiederhold et al., 2010), mineral precipitation (Smith et al., 2015), and evaporation (Estrade et al., 2009; Ghosh et al., 2013) have also been shown to cause significant MDF. While these processes commonly lead to a lower δ^{202}Hg in the product and a higher δ^{202}Hg in the residual pool of reactant, the degree of MDF varies depending on the reaction type and the extent of reaction.

Processes governing bioaccumulation, such as internal distribution in organisms (Kwon et al., 2013), tissue turnover (Kwon et al., 2016), and trophic transfer (Kwon et al., 2012), have been shown not to cause significant MDF. This has facilitated the use of mercury isotopes in fish muscle tissues for monitoring bioavailable mercury sources in many aquatic ecosystems (Balogh et al., 2015; Cransveld et al., 2017; Donovan et al., 2016; Lepak et al., 2018; Li et al., 2016; Kwon et al., 2014; Sackett et al., 2015; Sherman and Blum, 2013; Tsui et al., 2012, 2014; Yin et al., 2016). In contrast, a significantly higher δ^{202}Hg (by ~2‰) has been observed repeatedly in the tissues of birds (blood; Kwon et al., 2014; Tsui et al., 2018), bats (excrement; Kwon et al., 2015), seals (liver; Masbou et al., 2015), whales (muscle and liver; Masbou et al., 2018; Perrot et al., 2016), and in human hair (Du et al., 2018; Laffont et al., 2011; Li et al., 2014, 2016; Sherman et al., 2015a) compared to their respective dietary sources. The exact internal mechanism(s) responsible for the higher δ^{202}Hg in these tissues compared to dietary sources is still under debate. Given that microbial demethylation leads to a higher δ^{202}Hg in the reactant MMHg compared to the product IHg (Kritee et al., 2009), previous studies have hypothesized that internal demethylation followed by bioaccumulation of remaining MMHg with a higher δ^{202}Hg and excretion of a lighter δ^{202}Hg (IHg), may be responsible for the observed δ^{202}Hg values in these tissues.

2.2. Mass-independent fractionation

Mass-independent fractionation (MIF) is calculated using the difference between a measured δ^{xxx}Hg value and a value predicted based on MDF;

$$\Delta^{199}\mathrm{Hg} = \delta^{199}\mathrm{Hg} - (\delta^{202}\mathrm{Hg} \times 0.252) \quad (2)$$

$$\Delta^{200}\mathrm{Hg} = \delta^{200}\mathrm{Hg} - (\delta^{202}\mathrm{Hg} \times 0.5024) \quad (3)$$

$$\Delta^{201}\mathrm{Hg} = \delta^{201}\mathrm{Hg} - (\delta^{202}\mathrm{Hg} \times 0.752) \quad (4)$$

$$\Delta^{204}\mathrm{Hg} = \delta^{204}\mathrm{Hg} - (\delta^{202}\mathrm{Hg} \times 1.4930) \quad (5)$$

The MIF of odd mass number isotopes (^{199}Hg, ^{201}Hg) has been observed in soil, sediment, water, biota, and atmospheric samples (e.g., Blum et al., 2014). The nuclear volume effect (NVE) and the magnetic isotope effect (MIE) are the two mechanisms known to cause MIF of ^{199}Hg and ^{201}Hg. MIF via the NVE is dependent on the nuclear volume of the isotopes (Schauble, 2007) and occurs during both kinetic (non-photochemical Hg^{2+} reduction; Zheng and Hintelmann, 2010b) and equilibrium reactions (liquid-vapor evaporation; Estrade et al., 2009; Ghosh et al., 2013, mercury-thiol complexation; Wiederhold et al., 2010), resulting in a Δ^{199}Hg/Δ^{201}Hg slope of ~1.6. The MIE occurs during kinetic reactions and due to the nuclear spin of ^{199}Hg and ^{201}Hg (Buchachenko, 2001). The most well-known environmental processes producing MIE fractionation are aqueous IHg photoreduction and MMHg photodegradation (Bergquist and Blum, 2007; Zheng and Hintelmann, 2009). The Δ^{199}Hg value has been used to estimate the proportion of a particular mercury species that has undergone photochemical reactions, and the slope of Δ^{199}Hg/Δ^{201}Hg in the reactants and products has been used to distinguish between IHg photoreduction (Δ^{199}Hg/Δ^{201}Hg = 1.00 ± 0.02) and MMHg photodegradation (Δ^{199}Hg/Δ^{201}Hg = 1.36 ± 0.03) in natural samples (Bergquist and Blum, 2007). Biological samples mainly containing MMHg display Δ^{199}Hg/Δ^{201}Hg slopes of 1.2-1.3 (Balogh et al., 2015; Blum et al., 2013; Cransveld et al., 2017; Das et al., 2009; Gehrke et al., 2011a, 2011b; Kwon et al., 2013, 2014, 2015; Lepak et al., 2018; Li et al., 2016; Perrot et al., 2010, 2012; Senn et al., 2010; Sherman and Blum, 2013; Tsui et al., 2012, 2014; Yin et al., 2016). Samples mainly containing IHg such as rocks, minerals, soil, sediments, plants and atmospheric mercury display Δ^{199}Hg/Δ^{201}Hg slopes of ~1 (reviewed by Sonke, 2011; Yin et al., 2014).

Significant MIF anomalies of even mass number isotopes (^{200}Hg, ^{204}Hg) have been observed in atmospheric samples including Hg^0 and precipitation (Demers et al., 2013; Gratz et al., 2010; Rolison et al., 2013), open-ocean marine samples (fish and plankton; Motta et al., 2019), fish samples from large lakes (Lepak et al., 2015, 2018), and in the glass walls of mercury vapor compact fluorescent lamps (Mead et al., 2013). Positive Δ^{200}Hg values were first documented in precipitation containing oxidized Hg^{2+} species, and negative Δ^{200}Hg values have been observed in gaseous Hg^0 (Blum and Johnson, 2017; Chen et al., 2012; Demers et al., 2013; Gratz et al., 2010; Rolison et al., 2013). A recent study by Blum and Johnson (2017) compiled Δ^{200}Hg and Δ^{204}Hg of atmospheric samples and reported negative Δ^{204}Hg in conjunction with positive Δ^{200}Hg in precipitation samples with a Δ^{200}Hg/Δ^{204}Hg slope of ~-0.5. Since photoreduction of aqueous Hg^{2+} has not been shown to induce MIF of the even mass number isotopes (Bergquist and Blum, 2007), the even mass number MIF anomalies are speculated to be caused by photo-oxidation of gaseous Hg^0 (Chen et al., 2012). In the natural environment, oxidation of Hg^0 in the tropopause is regarded to be the dominant mechanism responsible for the observed Δ^{200}Hg in atmospheric samples (Cai and Chen, 2016; Chen et al., 2012). Given that laboratory photo-oxidation experiments have shown relatively small changes in Δ^{200}Hg, further studies are required to verify the environmental processes leading to the observed Δ^{200}Hg values in natural samples (Sun et al., 2016a; Sun et al., 2019).

2.3. Isotopic mixing

Isotopic mixing represents a process in which mercury sources or environmental pools with distinct mercury isotope ratios (end members) mix to varying degrees. Binary and tertiary mixing models have been employed for atmospheric samples (i.e., air mass contribution, e.g., Fu et al., 2016) as well as in sediments of streams, rivers, and coastal regions. Mixing models can estimate the relative contributions of, for example, mercury from atmospheric background and from an anthropogenic point source (e.g., mine tailings, historical industrial activities, chemical manufacturing or ash spills; Balogh et al., 2015; Bartov et al., 2013; Feng et al., 2010; Foucher and Hintelmann, 2009; Meng et al., 2019; Yin et al., 2013c; Donovan et al., 2014; Washburn et al., 2017). Using binary mixing as an example, the relative contribution of two mercury sources can be estimated as follows;

$$^{XXX}Hg_{mixture} = {}^{XXX}Hg_{source1} \times f_{source1} + {}^{XXX}Hg_{source2} \times f_{source2} \quad (6)$$

$$f_{source1} + f_{source2} = 1 \quad (7)$$

where ^{XXX}Hg represents either $\delta^{202}Hg$, $\Delta^{199}Hg$, or $\Delta^{200}Hg$, and f represents the fraction of each mercury source or end member.

Recent studies have also employed mixing models to estimate the relative contribution of multiple environmental pools of mercury as well as natural processes governing mercury input to ecosystems (e.g., Demers et al., 2013; Enrico et al., 2016; Jiskra et al., 2017; Kwon et al., 2015; Woerndle et al., 2018). For instance, Demers et al. (2013) estimated the relative contribution of precipitation, litterfall, and mineral soil to a Wisconsin forest floor (U.S.A). A study by Woerndle et al. (2018) used mercury isotope ratios in stream water to distinguish between the relative importance of atmospheric mercury input pathways of wet versus dry deposition. In other studies, the relative contribution of precipitation-derived (Hg^{2+} deposited in the form of precipitation) versus litter-derived (Hg^0 taken up by foliage and sequestered into soil) mercury runoff to adjacent aquatic ecosystems has been estimated using simple mixing models (Kwon et al., 2015; Jiskra et al., 2017).

3. Large-scale evaluation

3.1. Atmosphere

3.1.1. Total gaseous mercury

Mercury isotopic compositions of atmospheric total gaseous mercury (TGM), which is the sum of Hg^0 and Hg^{2+}, are compiled from the literature and represent samples collected from various locations in the U.S.A, China, and France (Table A.1). While the measurements are highly skewed towards these three countries, the TGM samples display a wide range in $\delta^{202}Hg$ (-3.88 to +1.11 ‰) and a relatively small range in $\Delta^{199}Hg$ (-0.41 to +0.19 ‰; Table A.1). As illustrated in Fig. 1A, TGM evaded from land and ocean surfaces (referred to as "surface evasion") and TGM collected from relatively remote regions without significant point-source anthropogenic mercury emissions (referred to as "background") are characterized by negative $\Delta^{199}Hg$ and $\Delta^{200}Hg$ values, and both negative and positive $\delta^{202}Hg$ values, respectively. TGM collected from regions with significant anthropogenic mercury emission sources (referred to as "urban-industrial") are characterized by near-zero to positive $\Delta^{199}Hg$ and $\Delta^{200}Hg$ values, and highly negative $\delta^{202}Hg$ values.

The negative $\Delta^{199}Hg$ and $\Delta^{200}Hg$ values observed in the background and surface evaded TGM can be explained by a higher Hg^0 and a lower Hg^{2+} contribution (Fig. 2A, B). TGM samples collected from background sites are comprised of mostly Hg^0 (> 75%; Pacyna et al., 2003) compared to TGM emitted by local anthropogenic emissions (Hg^0:Hg^{2+}: Hg_P =50:40:10; Pacyna et al., 2003), and they represent mercury that has undergone long-range transport and global mixing during which the isotopic compositions of TGM have been altered extensively by photochemical processes. The negative $\Delta^{199}Hg$ in the background TGM (-0.22 to -0.01‰) is a result of Hg^{2+} photoreduction

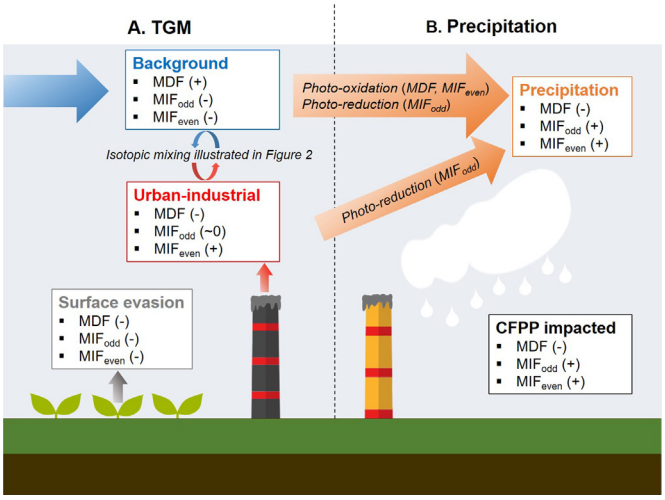

Fig. 1. MDF ($\delta^{202}Hg$), MIF_{odd} ($\Delta^{199}Hg$), and MIF_{even} ($\Delta^{200}Hg$) of atmospheric TGM and precipitation samples and the processes resulting in isotopic mixing (background and urban-industrial TGM) and fractionation (photochemical processes shown in orange arrows). "CFPP" refers to precipitation impacted by coal-fired power plants.

(leading to more negative $\Delta^{199}Hg$ in the product Hg^0) occurring in soil (Sonke, 2011; Sun et al., 2019) and water surfaces or in cloud droplets (Bergquist and Blum, 2007; Gratz et al., 2010), and display values similar to those re-emitted from ocean waters and rice paddy surfaces as Hg^0 (-0.41 to -0.03‰; Fig. 2A). The $\Delta^{200}Hg$ values used to differentiate between oxidized Hg^{2+} and gaseous Hg^0 (see Section 2.2) also show lower $\Delta^{200}Hg$ (-0.11 to 0.01‰) in the background and surface evaded TGM compared to those collected in urban-industrial sites ($\Delta^{200}Hg$ = -0.04 to 0.06‰; Fig. 2B).

The $\delta^{202}Hg$ of the background (-0.39 to 0.93‰) and surface evaded TGM (-3.88 to -0.33‰) are mostly positive and exclusively negative values, respectively (Fig. 2A). The positive $\delta^{202}Hg$ of the background TGM may be explained by the preferential uptake of lighter isotopes by vegetation during long-range transport. On a global basis, vegetation has been estimated to take up ~2500 Mg/year of Hg^0 from the atmosphere (Obrist et al., 2018). In a Wisconsin forest, Demers et al. (2013) observed a large MDF during Hg^0 uptake by foliage (-2 to -4‰), leaving the residual Hg^0 with positive $\delta^{202}Hg$ values. The negative $\delta^{202}Hg$ observed in the surface evaded TGM (crosses from Fig. 2A) is thought to reflect photoreduction followed by Hg^0 volatilization, further leading to negative $\delta^{202}Hg$ in the volatilized Hg^0. For instance, Rolison et al. (2013) collected TGM ~2 m above the sea level at Grand Bay, Mississippi, U.S.A. By coupling their results with air mass back trajectories, the authors inferred highly negative $\delta^{202}Hg$ values (< -2 ‰) in TGM transported via marine air masses compared to those transported via inland air masses ($\delta^{202}Hg$ > -2 ‰; black crosses from Fig. 2A). Recent studies that have characterized the isotopic compositions of TGM samples that are known to be influenced by mercury evaded from the marine surface (shaded box from Fig. 2A) have measured similar ranges as with the background TGM ($\delta^{202}Hg$= -1.63 to 0.91‰; $\Delta^{199}Hg$= -0.30 to -0.02‰). Demers et al. (2015) suggested that this reflects mixtures of background TGM and TGM that has undergone photoreduction and subsequent volatilization from the marine surface. The fact that TGM samples influenced by mercury evaded from the marine surface have similar isotopic compositions with background TGM suggests that the identification of re-emitted or legacy mercury sources from the global atmospheric mercury pool may be difficult.

Urban-industrial TGM was collected from Beijing and Guiyang, China and from Chicago, U.S.A. and displays near-zero $\Delta^{199}Hg$ (-0.16 to 0.15‰) and lower $\delta^{202}Hg$ (-2.03 to 1.11‰) compared to background TGM (Fig. 2A). The $\Delta^{200}Hg$ values are near-zero to positive (-0.04 to

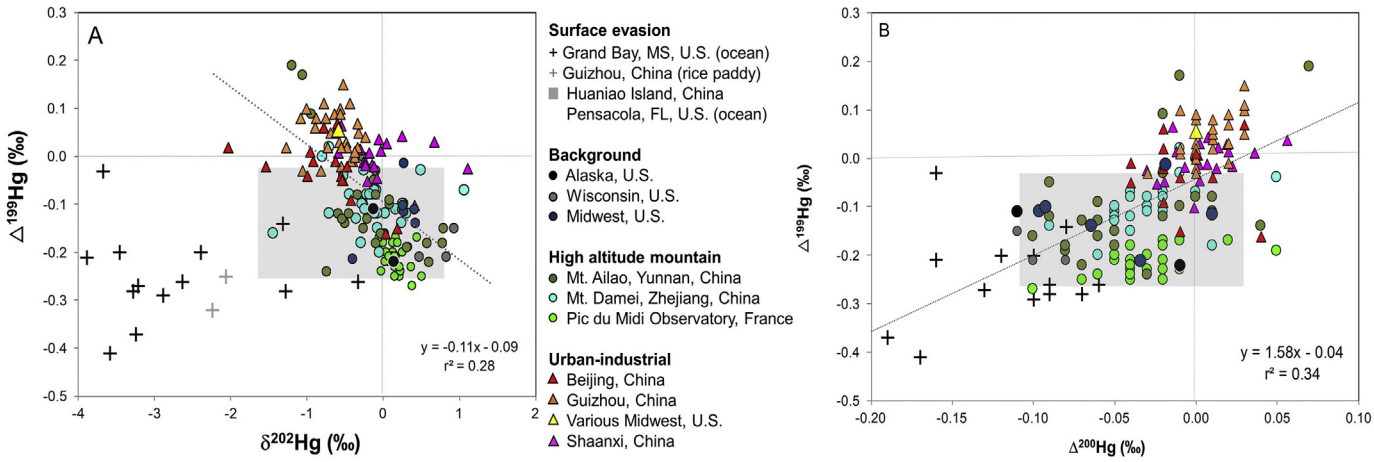

Fig. 2. δ^{202}Hg and Δ^{199}Hg values (A), and Δ^{200}Hg and Δ^{199}Hg values (B) of TGM samples. TGM samples are categorized by surface evasion (cross and shaded box), background (circle), high altitude mountain (circle), and urban-industrial sites (triangle), and by location (China, France, U.S.A). The dotted line in panel A represents a linear regression between δ^{202}Hg and Δ^{199}Hg values of background, high altitude mountain, and urban-industrial TGM. The solid line in panel B represents a linear regression between Δ^{200}Hg and Δ^{199}Hg values of background, high altitude mountain, surface evasion, and urban-industrial TGM.

0.06‰; Fig. 2B), suggesting a higher proportion of Hg^{2+} in TGM influenced or emitted from anthropogenic point sources. The δ^{202}Hg and Δ^{199}Hg of these TGM samples are similar to coal used in Beijing (δ^{202}Hg; -1.42 ± 0.37‰, Δ^{199}Hg; 0.05 ± 0.12‰), Guiyang (δ^{202}Hg; -1.00 ± 0.27‰, Δ^{199}Hg; -0.03 ± 0.04‰), and Chicago (δ^{202}Hg; -1.52 ± 0.37‰, Δ^{199}Hg; -0.09 ± 0.08‰), respectively (reviewed by Sun et al., 2014, 2016b). Slightly higher δ^{202}Hg observed in the TGM of Shannxi, China (Fig. 2A) is also consistent with higher δ^{202}Hg of coal used in this location, as suggested by the authors (Shaanxi; δ^{202}Hg; -0.67 ± 0.14‰, Δ^{199}Hg; -0.05 ± 0.02‰; Xu et al., 2017). Sun et al. (2013) documented a significant MDF during mercury speciation in the flue gas stream in coal-fired power plants (CFPP), resulting in more positive δ^{202}Hg in the emitted Hg^0 compared to Hg^{2+} and Hg_P. While mercury emitted from CFPPs contains large proportions of Hg^{2+} and Hg_P (Pacyna et al., 2003), atmospheric mixing of anthropogenic emission sources with background TGM with a slightly higher δ^{202}Hg may result in similar values.

It can be seen from Fig. 2A and Fig. 2B that TGM collected from high altitude mountains have wide ranges in δ^{202}Hg (-1.43 to 1.07‰), Δ^{199}Hg (-0.27 to 0.19‰), and Δ^{200}Hg (-0.10 to 0.07‰), consistent with mixing between the background and urban-industrial TGM. Fu et al. (2016) measured mercury isotopic compositions of TGM at the high elevation site of Pic du Midi Observatory, France originating from two air masses (Fig. 2A). The study documented significantly more positive δ^{202}Hg in TGM originating from the North Atlantic Ocean free troposphere and characterized by a low CO concentration (indicative of human activities) compared to anthropogenically influenced European air masses with high CO concentration, resulting in an overall wider range of δ^{202}Hg. Overall, a linear regression between δ^{202}Hg and Δ^{199}Hg and between Δ^{200}Hg and Δ^{199}Hg of TGM collected from urban-industrial and background sites of various locations of the world indicates that we can discern anthropogenic influences and mercury speciation within TGM. We suggest that future studies should characterize the isotopic compositions of TGM emitted or influenced by other anthropogenic emission sources (i.e., cement production, waste incineration, smelting) and those re-emitted from the land and ocean surfaces.

3.1.2. Precipitation

Mercury isotopic compositions of precipitation obtained from various locations of the U.S.A., Canada, and China (Table A.1) are characterized by negative MDF, and both positive Δ^{199}Hg and Δ^{200}Hg, which are opposite to those of the background TGM (Fig. 1B). When compared to urban-industrial TGM, the precipitation samples have similarly negative δ^{202}Hg and positive Δ^{200}Hg but more positive Δ^{199}Hg (Fig. 1B). Atmospheric redox processes appear to explain the differences in MDF and MIF between the TGM and precipitation samples. Mercury in precipitation is mostly comprised of Hg^{2+} and anthropogenic emission sources have been shown to emit a substantial proportion of Hg^{2+} that is characterized by negative δ^{202}Hg (Fig. 2A). As for the background TGM comprised mainly of Hg^0, photo-oxidation via chlorine (but not bromine) has been shown to generate Hg^{2+} with a lower δ^{202}Hg and a higher Δ^{200}Hg compared to Hg^0 based on laboratory studies (Sun et al., 2016a). Whether mercury is emitted as Hg^{2+} or has undergone photo-oxidation processes, it typically associates with cloud droplets and undergoes photoreduction, which results in an enrichment of Δ^{199}Hg and δ^{202}Hg in the remaining Hg^{2+} in precipitation (Gratz et al., 2010; Fig. 1B).

The extent of photochemical oxidation can also be evaluated over a large spatial scale via Δ^{200}Hg and Δ^{204}Hg values of precipitation. A previous study documented increasing trends in precipitation Δ^{200}Hg (between 0 to 1.30‰) with increasing latitude (25 to 45°N latitude; Cai and Chen, 2015). This pattern was found to be consistent with Chen et al. (2012), who documented significant positive Δ^{200}Hg (0.18 to 0.74‰) in precipitation collected from Peterborough, Canada when the air masses originated from the high Arctic instead of continental North America. The authors suggested that atmospheric mercury oxidation in the tropopause, which occurs at a lower altitude (i.e., 6000m) at higher latitudes, is responsible for elevated Δ^{200}Hg in precipitation. Given that Δ^{200}Hg and Δ^{204}Hg anomalies occur simultaneously and at Δ^{200}Hg/Δ^{204}Hg ratios of ~-0.5 (Blum and Johnson, 2017), we compiled Δ^{200}Hg and Δ^{204}Hg values for precipitation collected from a wider range of locations that are now published (Table A.1) and observed a Δ^{200}Hg/Δ^{204}Hg ratio of ~-0.4 ($r^2 = 0.30$, $p < 0.05$). The Δ^{200}Hg/Δ^{204}Hg ratios from Blum and Johnson (2017) and this study are both obtained from a linear regression between Δ^{200}Hg and Δ^{204}Hg values of averaged precipitation samples of each study location. The Δ^{200}Hg/Δ^{204}Hg ratio regressed over individual data points (not the averages of each study location) shows a lower value of -0.2 as illustrated in Fig. 3B ($r^2 = 0.20$, $p < 0.05$). The precipitation samples collected from sites designated as background (blue circles; Fig. 3B) displayed a slightly higher Δ^{200}Hg/Δ^{204}Hg ratio compared to those collected from semi-rural (yellow-orange circles) and urban sites (pink-red triangles), suggesting a potential dilution effect by anthropogenic sources.

In regards to source differentiation, precipitation collected at urban (local point sources exist), semirural (nearby local point sources plus long-range transport), and background sites (no nearby local point sources) as well as those collected shipboard north of Oahu and on the

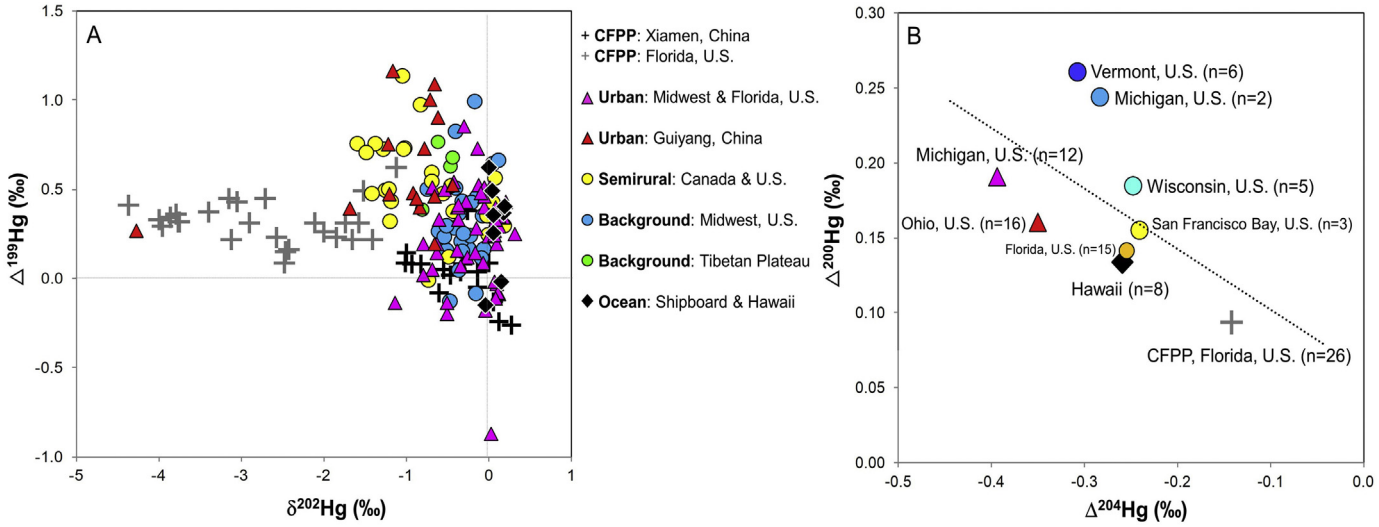

Fig. 3. δ^{202}Hg and Δ^{199}Hg values (A), and average Δ^{204}Hg and Δ^{200}Hg values (B) of precipitation samples. Precipitation samples designated as CFPP (crosses) and ocean (diamonds) are those impacted by coal-fired power plants and those collected shipboard north of Oahu and on the Island of Hawaii, respectively. Precipitation samples are further categorized by background (circle), semirural (circle) and urban sites (triangle) and by location (China, Canada, U.S.A.). The dotted line in panel B represents a linear regression between Δ^{204}Hg and Δ^{200}Hg values of individual (not averages by site) precipitation samples (slope = -0.2, r^2 = 0.20, $p < 0.05$).

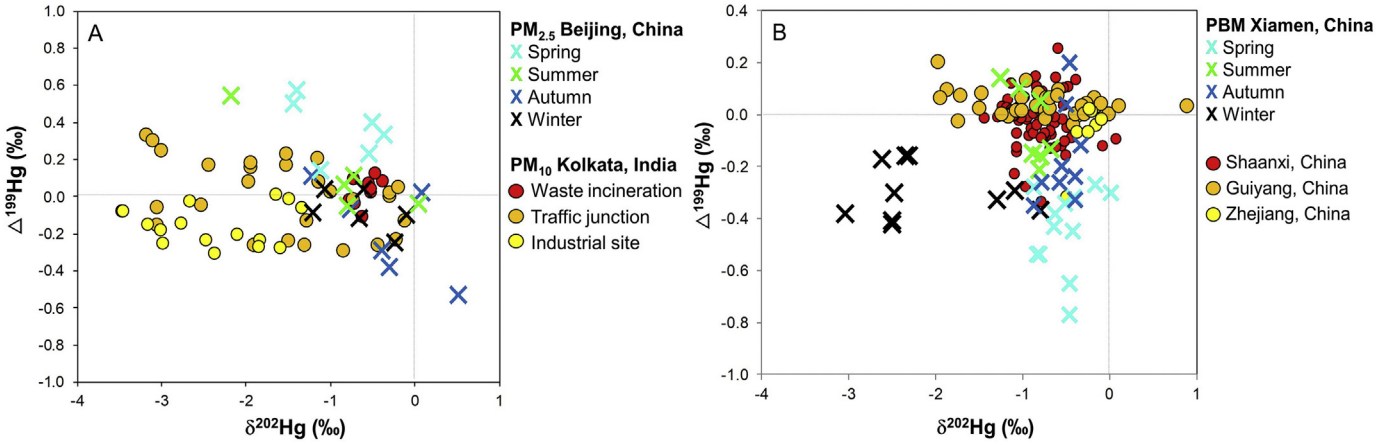

Fig. 4. δ^{202}Hg and Δ^{199}Hg values of $PM_{2.5}$ and PM_{10} (A) and total PBM (B) collected from China and India.

Island of Hawaii (referred to as "ocean" samples) do not exhibit distinct δ^{202}Hg and Δ^{199}Hg values (Fig. 3A). Gratz et al. (2010) compared mercury isotopic compositions of precipitation collected from rural (Dexter, MI), semi-rural (Holland, MI), and urban sites (Chicago, IL) from the Midwest, U.S.A. and observed no significant differences. One reason for this is that precipitation reflects mixtures of locally emitted mercury and mercury that has undergone redox reactions in the atmosphere during regional transport. Various atmospheric processes including photoreduction, oxidation, adsorption, and desorption can lead to MDF, MIF_{odd} and MIF_{even} in precipitation and obscure the source signature. In contrast, Sherman et al. (2012) first discovered that precipitation collected downwind from a CFPP in Florida, U.S.A. during storm events was characterized by particularly negative δ^{202}Hg (-4.37 to -1.12‰; grey crosses from Fig. 3A). The highly negative δ^{202}Hg is consistent with Hg^{2+} and Hg_P emitted from a CFPP (Sun et al., 2013). Recent measurements of precipitation impacted by a CFPP in Xiamen, China had higher δ^{202}Hg (-1.02 to 0.28‰) and slightly lower Δ^{199}Hg values (-0.26 to 0.38‰) compared to those observed in Florida, U.S.A. (black crosses in Fig. 3A). The authors suggested that the near-zero δ^{202}Hg observed in precipitation may be caused by mixtures of mercury transported from long-distances, atmospheric processes resulting in isotope fractionation, and mercury emitted via the combustion of coal with high δ^{202}Hg values (-1.07‰; Huang et al., 2018). Additional studies will be needed to better understand sources and processes resulting in the differences in the mercury isotopic composition of precipitation, particularly when it is impacted by the largest mercury emission sources, which are CFPPs. Meanwhile, measurements of Δ^{200}Hg and Δ^{204}Hg values in precipitation provide an important opportunity to monitor spatial differences in the extent of photochemical oxidation of mercury in the atmosphere, which is the major process governing atmospheric mercury deposition.

3.1.3. Hg_P

The isotopic compositions of Hg_P represent local to regional anthropogenic mercury sources given their short lifetime in the atmosphere (days to weeks; Schroeder and Munthe, 1998). Studies that have characterized Hg_P isotopic compositions collected either total Hg_P (Huang et al., 2018; Xu et al., 2017; Yu et al., 2016), $PM_{2.5}$, or PM_{10} (Das et al., 2016; Huang et al., 2016), and at locations experiencing severe air-borne particulate matter (PM) pollution including urban areas in China and India (Table A.1). The isotopic compositions of $PM_{2.5}$ shown in Fig. 4A are those collected from Beijing and demonstrate a moderate seasonal variation in δ^{202}Hg and Δ^{199}Hg (autumn < winter < summer < spring). Huang et al. (2016) suggested that large-scale biomass burning and coal combustion, which have relatively negative Δ^{199}Hg in the source material, explain the low Δ^{199}Hg

observed in the autumn (-0.53 to 0.11‰) and winter (-0.25 to 0.04‰), respectively. Backward trajectories of air masses confirmed that $PM_{2.5}$ collected during spring and summer seasons was from regional air mass transport and the higher degree of photoreduction during warmer seasons was used to explain the elevated $\Delta^{199}Hg$ (-0.05 to 0.57‰). Das et al. (2016) characterized the isotopic compositions of PM_{10} from a nearby municipal landfill, an industrial site, and a traffic junction in Kolkata, India (Fig. 4A). The higher $\delta^{202}Hg$ (-0.78 to -0.39‰) and low $\Delta^{199}Hg$ (-0.11 to 0.12‰) of PM_{10} collected from a municipal waste incinerator were explained by volatilization of liquid mercury used in mercury-added products, which have near-zero $\delta^{202}Hg$ and $\Delta^{199}Hg$ (Laffont et al., 2011). The lower $\delta^{202}Hg$ and variable $\Delta^{199}Hg$ of PM_{10} from an industrial site ($\delta^{202}Hg$ = -3.48 to -1.34‰, $\Delta^{199}Hg$ = -0.31 to 0.01‰) and from a traffic junction ($\delta^{202}Hg$ = -3.18 to -0.12‰, $\Delta^{199}Hg$ = -0.30 to 0.33‰) were attributed to mixtures of mercury emitted from waste incineration, vehicle emissions, and coal combustion.

Total Hg_P collected from an urban area of Shaanxi, Guiyang, and at a high elevation site of Zhejiang province, China (Fig. 4B; Xu et al., 2017; Yu et al., 2016) reflect influences from coal combustion (Shaanxi coal; $\delta^{202}Hg$; -0.67 ± 0.14‰, $\Delta^{199}Hg$; -0.05 ± 0.02‰; Guiyang coal; $\delta^{202}Hg$; -1.00 ± 0.27‰, $\Delta^{199}Hg$; -0.03 ± 0.04‰; reviewed in Sun et al., 2016b). These studies also collected TGM samples from the same site (Fig. 2A; Xu et al., 2017; Yu et al., 2016) and found slightly more positive $\delta^{202}Hg$ in TGM compared to the total Hg_P, consistent with MDF in the flue gas of CFPPs (Sun et al., 2013). The total Hg_P collected from Xiamen, China displayed wide ranges and somewhat overlapping $\delta^{202}Hg$ and $\Delta^{199}Hg$, representing the influence of varying mercury sources via differences in seasonal air masses (Huang et al., 2018; Fig. 4B). The isotopic composition of total Hg_P collected during the winter season ($\delta^{202}Hg$ = -3.05 to -0.80‰, $\Delta^{199}Hg$; -0.42 to -0.16‰) was attributed to a cold Siberian airmass carrying the emissions from biomass burning to the north. This is consistent with the negative $\Delta^{199}Hg$ but inconsistent with relatively high $\delta^{202}Hg$ observed in $PM_{2.5}$ influenced by biomass burning (Huang et al., 2016; black crosses from Fig. 4A). The highly negative $\delta^{202}Hg$ observed here is more similar to the negative $\delta^{202}Hg$ values reported for vegetation (-2.53 to -1.05‰; Demers et al., 2013). The total Hg_P collected during the spring season showed highly negative $\Delta^{199}Hg$ (-0.77 to -0.27‰), which was explained by atmospheric oxidation of Hg^0, causing the product Hg^{2+} to display negative $\Delta^{199}Hg$. Remaining samples collected during summer ($\delta^{202}Hg$ = -1.26 to -0.68‰, $\Delta^{199}Hg$ = -0.21 to 0.14‰) and fall seasons ($\delta^{202}Hg$ = -0.88 to -0.34‰, $\Delta^{199}Hg$ = -0.35 to 0.20‰) are within the ranges of those collected from Guiyang and Shaanxi (Xu et al., 2017; Yu et al., 2016), suggesting the influence of local coal combustion. While several recent studies have attempted to decipher seasonal differences in Hg_P isotopic compositions, the overlapping isotopic compositions of local mercury emission sources and fractionation due to complex atmospheric processes present a number of ambiguities in regards to the interpretation of the observed Hg_P isotopic compositions. We suggest that the coupling of backward trajectories of air masses and detailed characterization of source materials (i.e., local coal and biomass used for heating) will be necessary to fully understand the seasonal differences in mercury sources on local and regional scales. Studies that assess Hg_P isotope ratios in regions other than China and India will also need to evaluate the feasibility of Hg_P isotope ratios for source apportionment.

3.2. Terrestrial

3.2.1. Forest ecosystems

Mercury exchange between forest and atmospheric reservoirs is tightly coupled through Hg^0 uptake via foliage and re-emission from soil and foliage. As illustrated in Fig. 5, various biogeochemical processes have been shown to cause significant MDF and small MIF_{odd} of atmospheric mercury in forest ecosystems. Foliage samples collected in a Wisconsin forest as well as foliage and fresh litter samples collected at various forest sites across the U.S.A. show relatively narrow ranges in $\delta^{202}Hg$ (-2.67 to -1.64‰) and $\Delta^{199}Hg$ (-0.47 to 0.3‰; Fig. 6A). Foliage is thought to accumulate primarily Hg^{2+} following stomatal uptake of Hg^0 and oxidation within leaves. The process of reactive surface uptake has also been observed in the Arctic snowpack (Douglas and Blum, 2019). Thus, forest litter also represents predominantly Hg^0 taken up via foliage and oxidized to Hg^{2+} as well as some Hg_P deposited on leaf surfaces via dry deposition and throughfall (Ericksen et al., 2003; Rea et al., 2002). The ranges of foliage and litter $\delta^{202}Hg$ and $\Delta^{199}Hg$ are, however, inconsistent with the ranges of TGM collected from background sites (Fig. 2A). Demers et al. (2013) first observed a much lower $\delta^{202}Hg$ in foliage (-2 to -4‰) compared to TGM collected from a Wisconsin forest, and attributed this to a preferential uptake of lighter mercury isotopes by the foliage tissues. Lower $\Delta^{199}Hg$ observed in foliage (-0.2‰ shift) compared to TGM at the Wisconsin forest was attributed to the uptake of mercury that had already undergone photoreduction from the atmosphere or photoreduction in foliage (Fig. 5).

A number of recent studies have reported that $\Delta^{199}Hg$ of foliage and litter samples can be used to distinguish between the relative contribution of various atmospheric mercury sources on local to regional scales (Wang et al., 2016; Yu et al., 2016; Yuan et al., 2019). In general, the $\Delta^{199}Hg$ values observed in foliage and litter samples have been found to be consistent with either TGM collected from background sites characterized by negative $\Delta^{199}Hg$ or those from urban-industrial sites with near-zero $\Delta^{199}Hg$ (Fig. 2A). For instance, Yu et al. (2016) observed a significant positive relationship between total mercury concentration and $\Delta^{199}Hg$ in litter samples collected from Mountain Ailao (Yunnan, China) and Mountain Damei (Zhejiang, China). The authors suggested that litter samples that were once foliage and have taken up anthropogenic TGM are characterized by high mercury concentrations and near-zero $\Delta^{199}Hg$, whereas litter samples influenced by background TGM are characterized by low mercury concentration and slightly negative $\Delta^{199}Hg$ (-0.38 to -0.2‰). Wang et al. (2016) also reported a significant negative relationship between elevation and $\Delta^{199}Hg$ in litter samples collected from the Tibetan Plateau and suggested that litter samples collected at higher elevations (3700-4300m) are more likely to take up background TGM (into foliage) compared to those at lower elevations (3100-3600m) with higher anthropogenic influences.

In contrast to $\Delta^{199}Hg$, no particular source-relevant pattern has been reported for $\delta^{202}Hg$ in foliage and litter samples owing to the large MDF during Hg^0 uptake by foliage (Demers et al., 2013), which masks more subtle isotopic signals. Interestingly, our large-scale data compilation shows lower $\delta^{202}Hg$ in litter samples collected from China (-4.18 to -0.95‰; Yu et al., 2016; Wang et al., 2016) compared to litter and foliage samples collected in the U.S.A (-2.67 to -1.64‰; Zheng et al., 2016; Fig. 6A), consistent with the observation made in a recent study that modeled the distribution of mercury isotope ratios in various surface reservoirs (Sun et al., 2019). We suggest that the influence of anthropogenic TGM may explain the low $\delta^{202}Hg$ in the Chinese litter samples. TGM collected from the same site as litter in China displayed more negative $\delta^{202}Hg$ (-1.19 to 0.80‰; Yu et al., 2016; Fig. 2A) compared to the background TGM. Considering the large MDF during Hg^0 uptake via foliage, the uptake of anthropogenically emitted TGM with negative $\delta^{202}Hg$ may impart highly negative $\delta^{202}Hg$ in the Chinese litter. It appears that foliage and litter samples may be good alternative tracers for anthropogenic mercury influences. We emphasize, however, that these studies are limited to only a few locations in the U.S.A. and China and further monitoring of TGM together with foliage mercury isotopic compositions at other locations will be necessary to precisely evaluate the widespread utility of foliage and litter for source tracing under the MC.

The $\delta^{202}Hg$ and $\Delta^{199}Hg$ values of the forest floor (soil O horizons) collected in Wisconsin (Demers et al., 2013) are higher compared to foliage (on average by 0.74‰ in $\delta^{202}Hg$ and by 0.12‰ in $\Delta^{199}Hg$) collected at the same sites (Fig. 6A). The higher $\delta^{202}Hg$ (-1.88 to

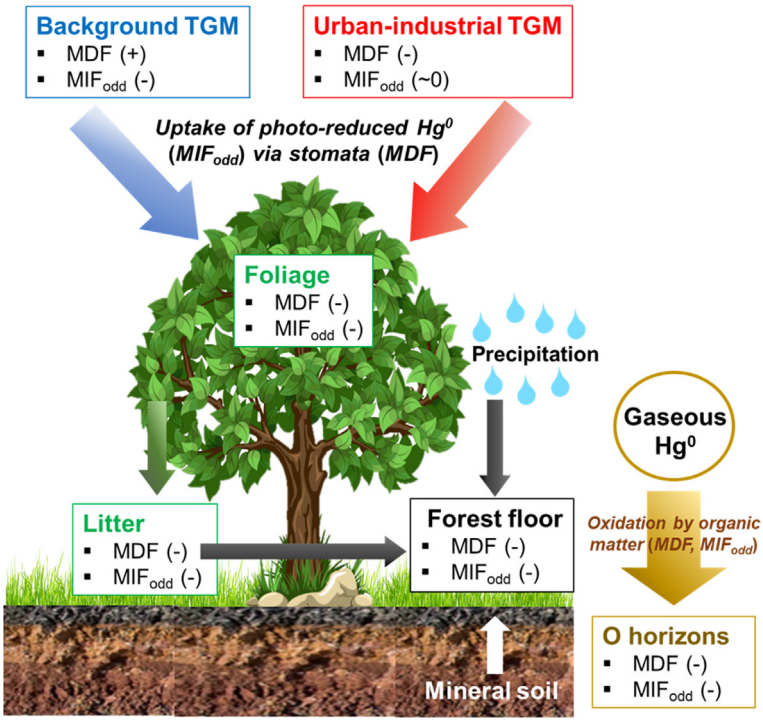

Fig. 5. MDF (δ^{202}Hg) and MIF_{odd} (Δ^{199}Hg) of forest samples and the processes resulting in isotopic mixing (litter, mineral soil, and precipitation; grey and white arrows) and fractionation (Hg^0 uptake via stomata and oxidation by soil organic matter; OM).

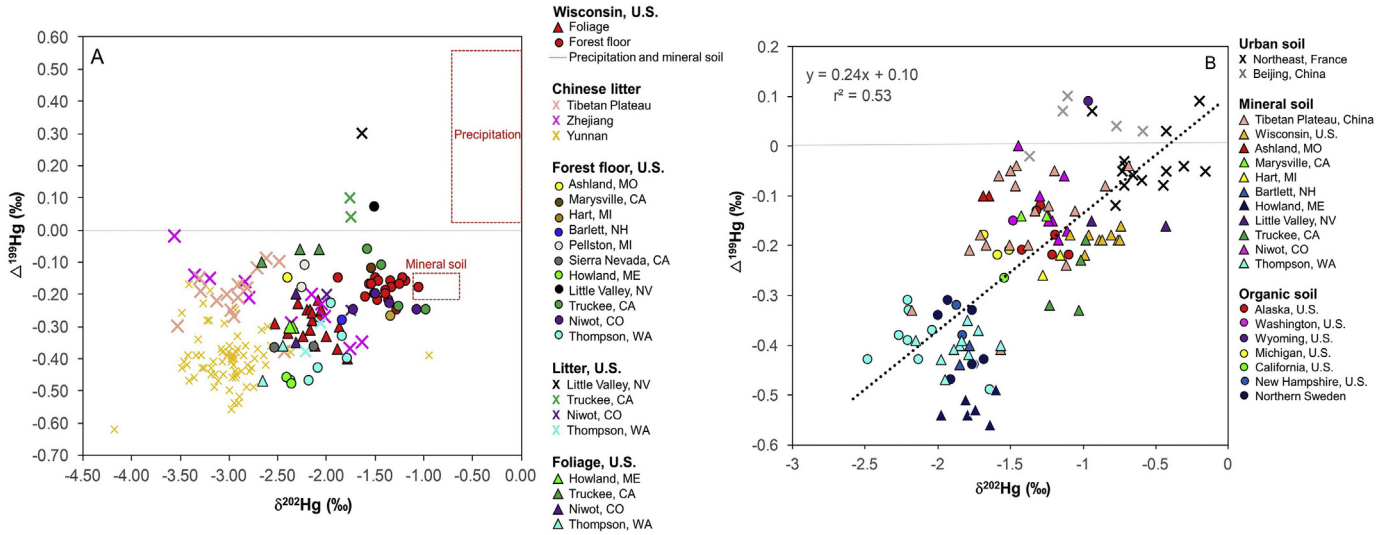

Fig. 6. δ^{202}Hg and Δ^{199}Hg values of forest samples (A), and various soils (B). Forest samples are categorized by foliage, litter, and forest floor and by location (U.S.A. and China). Red boxes in panel A represent the ranges of δ^{202}Hg and Δ^{199}Hg values of mineral soil and precipitation from Demers et al. (2013). Soil samples shown in panel B are categorized by urban, mineral, and organic soil reported from the U.S.A., France, and China. The dotted line in panel B represents a binary mixing between urban soil and soil with high organic matter content (% OM).

-1.05‰) and Δ^{199}Hg (-0.25 to -0.15‰) observed in the Wisconsin forest floor have been explained as a mixture of mercury originating from foliage (litterfall Hg^{2+}), precipitation (throughfall Hg^{2+}, Hg_P), and mineral soil (red symbols from Fig. 6A), as suggested by previous studies that considered only mercury concentrations (Rea et al., 2000). Using a tertiary mixing model, Demers et al. (2013) estimated that Hg^{2+} input to the forest floor via litterfall accounted for ~84% of the total mercury input. Large Hg^{2+} contributions via litterfall (~90%) have also been estimated using a mixing model in soil collected from boreal forests in Sweden and Norway (Jiskra et al., 2015, 2017). At a few locations across U.S.A. forests, Zheng et al. (2016) also observed higher δ^{202}Hg (-2.41 to -0.98‰) but slightly lower Δ^{199}Hg (-0.48 to 0.07‰) in the forest floor (soil O horizons) compared to litter samples collected at the same sites (Fig. 6A). While organic soil horizons showed no further changes in Δ^{199}Hg, δ^{202}Hg showed small but significant increases with soil depth (Zheng et al., 2016). This pattern is consistent with a recent experimental study of dark abiotic Hg^0 oxidation via thiols and natural soil humic acid in which the product Hg^{2+} was found to have a higher δ^{202}Hg and a slightly lower Δ^{199}Hg caused by equilibrium MDF and the NVE, respectively (Zheng et al., 2019). We however note that the dark abiotic Hg^0 oxidation experiment (Zheng et al., 2019) was conducted in aqueous solution using dissolved Hg^0 and may not reflect the oxidation of gaseous atmospheric Hg^0 by natural soil humic acid. Another possibility is that abiotic Hg^{2+} reduction by natural

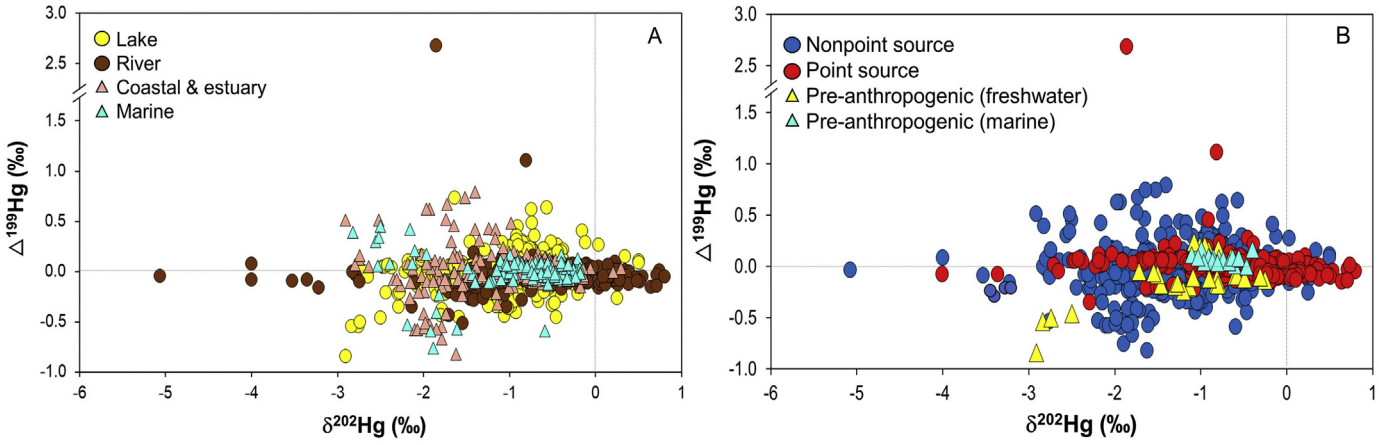

Fig. 7. δ^{202}Hg and Δ^{199}Hg values of sediments categorized by ecosystem type (A), and the degree of anthropogenic influence (B).

organic matter in soil followed by Hg^0 re-emission into the atmosphere can lead to an enrichment of δ^{202}Hg in soil (Jiskra et al., 2015). Further studies will be needed to understand the mechanism responsible for the observed δ^{202}Hg shifts in the forest floor and organic soil horizons.

3.2.2. Various soil types

Apart from the forest floor soil samples discussed above, we further compiled mercury isotope data that was identified by "soil type" from the literature (Table A.1). As illustrated in Fig. 6B, soil samples are categorized by organic (same as forest floor) and mineral soil (located beneath organic soil layers) both of which are from forests, and surface soil collected from urban-industrial regions (referred to as "urban soil") from Beijing, China, and Northeast, France (Table A.1). Decreasing trends in δ^{202}Hg and Δ^{199}Hg were observed from urban to mineral to organic soil. Demers et al. (2013) observed a similar decreasing trend in δ^{202}Hg from mineral soil to organic soil (same as forest floor) in a Wisconsin forest, and suggested that this follows a binary mixing between geogenic sources (i.e., crustal rocks) characterized by low % organic matter (OM) and an average δ^{202}Hg of ~ -0.6‰ (-1.70 to 1.61‰; Smith et al., 2008), and foliage characterized by high % OM and an average δ^{202}Hg of ~ -2.5‰ (-2.67 to -1.64‰; Fig. 6A). As for Δ^{199}Hg, geogenic sources and urban-industrial TGM (Fig. 2A) are characterized by near-zero to positive Δ^{199}Hg values, which explain the elevated Δ^{199}Hg in the mineral and urban soil. The negative Δ^{199}Hg observed in organic soil (high % OM) can be attributed to the uptake of atmospheric Hg^0 with negative Δ^{199}Hg (and its conversion to Hg^{2+}) (Fig. 2A) in foliage and the subsequent decay of foliage. In fact, we observed similar ranges in both δ^{202}Hg and Δ^{199}Hg between organic soil (Fig. 6B) and foliage samples (Fig. 6A) collected from various locations in the U.S.A. The urban soil δ^{202}Hg and Δ^{199}Hg were within the ranges of TGM collected from urban-industrial sites (Fig. 2A). This indicates that, while soil collected from forests dominantly reflects the influence of mercury delivered via foliage (litterfall), direct atmospheric deposition of mercury from anthropogenic emissions appears to explain the observed values in soil collected from urban sites with limited vegetative cover.

In the context of identifying factors influencing the uptake of atmospheric mercury, Zheng et al. (2016) suggested that mineral soil can be used to identify spatially variable processes affecting atmospheric mercury input and fate across forest ecosystems in the U.S.A. The lower Δ^{199}Hg (-0.56 to -0.35‰; Fig. 6B) and Δ^{200}Hg values (-0.05 to 0‰; not shown here), consistent with the isotopic compositions of Hg^0, were observed at more northern and wetter sites (Thompson, Washington; Bartlett, New Hampshire; and Howland, Maine) compared to drier and lower latitude sites in the U.S.A. (Hart, Michigan; Ashland, Missouri and Marysville, California; Δ^{199}Hg = -0.26 to -0.10‰, Δ^{200}Hg = 0.02 to 0.06‰). The authors suggested that vegetation in the wetter sites takes up higher amounts of atmospheric Hg^0 due to higher plant productivity and litterfall, as suggested previously by Obrist et al. (2014). In contrast, the reactive surface uptake may be limited in the drier sites due to decreased stomatal conductance for water conservation. High altitude sites such as Niwot Ridge, Colorado (3050m), Little Valley, Nevada (2011m), and Truckee, California (1767m) displayed elevated Δ^{199}Hg (-0.33 to 0‰; 6B), and the authors attributed this to the deposition of atmospherically oxidized mercury from the upper tropopause. Similar to foliage and litter samples, the utility of mineral soil for understanding climatic factors influencing the uptake of atmospheric mercury will require broader spatial scale assessments. Moreover, the fact that the mercury isotope ratios of various soil types are controlled primarily by the extent of vegetative cover suggests that the evaluation of anthropogenic mercury influences across a large spatial scale may be difficult.

3.3. Sediment

Mercury isotopic compositions of sediments are categorized by the type of aquatic ecosystem (Fig. 7A) and the degree of anthropogenic influence (Fig. 7B). A few riverine sediment samples collected from the Almaden, Spain mining district (Δ^{199}Hg = 1.11 to 2.68‰; Jiménez-Moreno et al., 2016) display anomalously high positive Δ^{199}Hg values, and a few riverine sediments collected from the Murray Brook Mine, Canada (δ^{202}Hg = -4.00 to -3.36‰; Foucher and Hintelmann, 2006) and from East Fork Poplar Creek, Tennessee, U.S.A. display highly negative δ^{202}Hg values (δ^{202}Hg = -5.07 to -3.53‰; Donovan et al., 2014). All three of these rivers are impacted by high levels of legacy industrial mercury pollution. Excluding samples from these locations, the remaining sediment isotope values compiled in this study, regardless of the ecosystem type, are within the ranges of -3.22 to 0.80‰ and -0.84 to 0.79‰ for δ^{202}Hg and Δ^{199}Hg, respectively. The sediments impacted by point sources of mercury exhibit a similar δ^{202}Hg range and a narrower Δ^{199}Hg range near zero, compared to those influenced by nonpoint mercury sources (Fig. 7B). The near-zero Δ^{199}Hg samples are consistent with metallic and liquid mercury extracted or used during mining and industrial processes (reviewed in Sun et al., 2016c) as well as TGM emitted from anthropogenic sources (Fig. 2A).

To further evaluate the isotopic differences among sediments that have been impacted by various point source activities, we divided sediments into those affected by a fly ash spill from a CFPP, metal smelters, chemical industries that use mercury as catalysts, metallic mercury spills, and mercury/gold mining. As illustrated in Fig. 8A, sediments impacted by fly ash and smelting activities have particularly wide ranges in both δ^{202}Hg and Δ^{199}Hg. The δ^{202}Hg (-1.63 to -0.10‰) of riverine sediments impacted by a fly ash spill from the Kingston, Tennessee CFPP, U.S.A. (Bartov et al., 2013) are consistent with fly ash

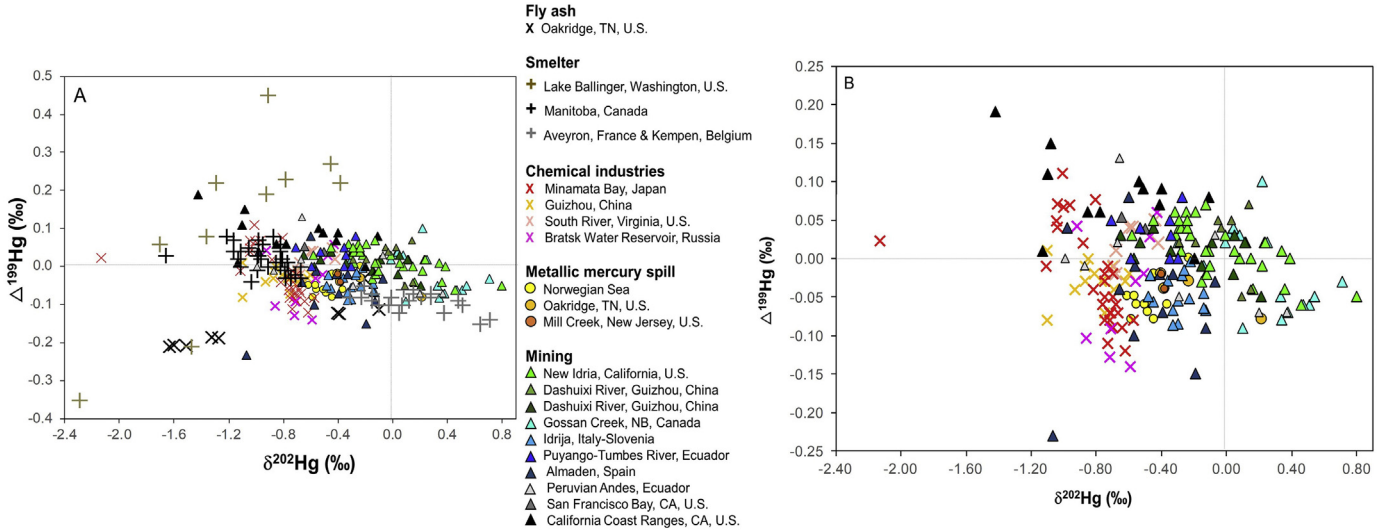

Fig. 8. δ^{202}Hg and Δ^{199}Hg values of sediments impacted by different types of point source activities as shown in the legend (A). Sediments impacted by chemical industries, metallic mercury spills, and mining activities are shown on an expanded scale in (B).

generated from Chinese CFPPs (δ^{202}Hg = -1.91 to -0.85‰; Sun et al., 2013). Lake sediments impacted by smelters in Washington, U.S.A. (-2.29 to -0.38‰; Gray et al., 2013) and Manitoba, Canada (-1.66 to -0.67‰; Ma et al., 2013) are much lower in δ^{202}Hg compared to riverine sediments impacted by smelters in Belgium and France (-0.31 to 0.71‰; Sonke et al., 2010; Fig. 8A). The riverine sediments contaminated by former zinc (Zn) smelters in Belgium and France are impacted by slag tailings effluents from high-temperature ZnS ore processing, leading to higher δ^{202}Hg values in slag tailings compared to the ZnS ores (Sonke et al., 2010). Lake sediments from Manitoba, Canada (Ma et al., 2013) and Washington, U.S.A. (Gray et al., 2013) are influenced by atmospherically deposited mercury from Cu-Zn smelters and Pb-Cu smelters, respectively. While the source of the elevated Δ^{199}Hg has not been fully elucidated, Gray et al. (2013) suggested that this is likely related to pre-existing MIF in the original ore, the smelting processes, and/or chemical modification during sediment deposition.

The remaining sediments impacted by chemical industries, mining activities (gold and mercury mining), and metallic mercury releases can be segregated by negative δ^{202}Hg (chemical industries; -0.77 ± 0.24‰), near-zero δ^{202}Hg (mining; -0.26 ± 0.59‰), and intermediate values between outputs from the chemical industry and mining activities (metallic mercury release; -0.39 ± 0.19‰), respectively (Fig. 8B). Sediments impacted by direct metallic mercury releases as well as metallic mercury used as a catalyst at Oak Ridge, Tennessee, U.S.A. show δ^{202}Hg and Δ^{199}Hg that are consistent with metallic mercury reported by previous studies (δ^{202}Hg = -0.28 ± 0.29‰; Laffont et al., 2011, Sun et al., 2016c). A study that estimated an isotopic end member of the effluent discharged from a chemical plant at Minamata Bay, Japan reported δ^{202}Hg of -0.69‰ and Δ^{199}Hg of -0.07‰ (Balogh et al., 2015). Washburn et al. (2017) observed similar δ^{202}Hg (-0.69 to -0.42 ‰) in the effluent discharged from a historic chemical plant that used mercury as a catalyst for acetate fiber production in South River, Virginia, U.S.A. Remaining sediments impacted by a chlor-alkali plant (Perrot et al., 2010) and a chemical industry that produced acetic acid (Feng et al., 2010) also show similar δ^{202}Hg values. Given that these sediments were collected from a wide range of environments (reservoir, river, lake, coastal), we suggest that industrial processes leading to MDF of mercury that is used as a catalyst, rather than biogeochemical processes in the sediment, are responsible for the negative δ^{202}Hg values. This is in agreement with the previous study that reported sediment mercury isotope ratios impacted by various types of industrial sources (Wiederhold et al., 2015).

The wide δ^{202}Hg range observed in sediments impacted by mining activities are due to 1) the wide δ^{202}Hg ranges in mercury-containing ores, 2) roasting processes leading to MDF in waste calcine, and 3) environmental processes leading to MDF in sediments (Fig. 8B). Smith et al. (2008) reported a wide δ^{202}Hg range (between -3.88‰ and 1.61‰) in mercury-containing rocks, ore deposits, and active spring deposits from a mercury mine in the California Coast Ranges. Hintelmann and Lu (2003) also observed a large δ^{202}Hg variation (between -1.73‰ and 1.33‰) in mercury ores collected from various locations across the world. High temperature roasting of mercury ores, a process used to extract metallic mercury, has been shown to cause significant MDF, resulting in a higher δ^{202}Hg in calcine deposits compared to volatilized Hg^0 (Gehrke et al., 2011a; Smith et al., 2014; Yin et al., 2013a, 2013b, 2013c). More recent studies have shown that incomplete roasting of mercury ores at mining sites can cause wide ranges in δ^{202}Hg (between -5.94‰ and 14.49‰; Smith et al., 2014). In addition, Wiederhold et al. (2013) observed higher δ^{202}Hg in more soluble mercury pools in calcine, compared to residual mercury sulfide phases, using sequential extraction methods. In regards to the environmental processes leading to MDF in sediments, Foucher et al. (2013) reported a progressive enrichment in sediment δ^{202}Hg with increasing distance away from the Murray Brooks Mine located in New Brunswick, Canada. The authors suggested that environmental processes such as reduction of suspended Hg^{2+} from the sediment and subsequent Hg^0 volatilization from the water column may have been responsible for the higher δ^{202}Hg in the downstream sediment. In the case of sediments impacted by ASGM activities, a recent study has observed consistent mercury isotope ratios between sediments located downstream of ASGM and mercury used during gold extraction (δ^{202}Hg = -0.71 to -0.27‰, near zero Δ^{199}Hg; Schudel et al., 2018). Another study observed relatively negative δ^{202}Hg (between -1.90 and -1.13‰) in sediments impacted by ASGM activities and suggested that runoff of soil influenced by ASGM may be a more important source to the sediments rather than mercury used during gold extraction (Adler Miserendino et al., 2018). In general, we find that sediments show relatively distinct δ^{202}Hg depending on the type of point mercury source influence. However the utility of sediment mercury isotope ratios for source monitoring across a large spatial scale has not been fully tested and we caution that isotopic values can be modified by a wide range of biogeochemical processes and anthropogenic activities. In Section 5, we discuss further how sediment mercury isotope ratios can be used to evaluate sources responsible for mercury contamination at a local scale.

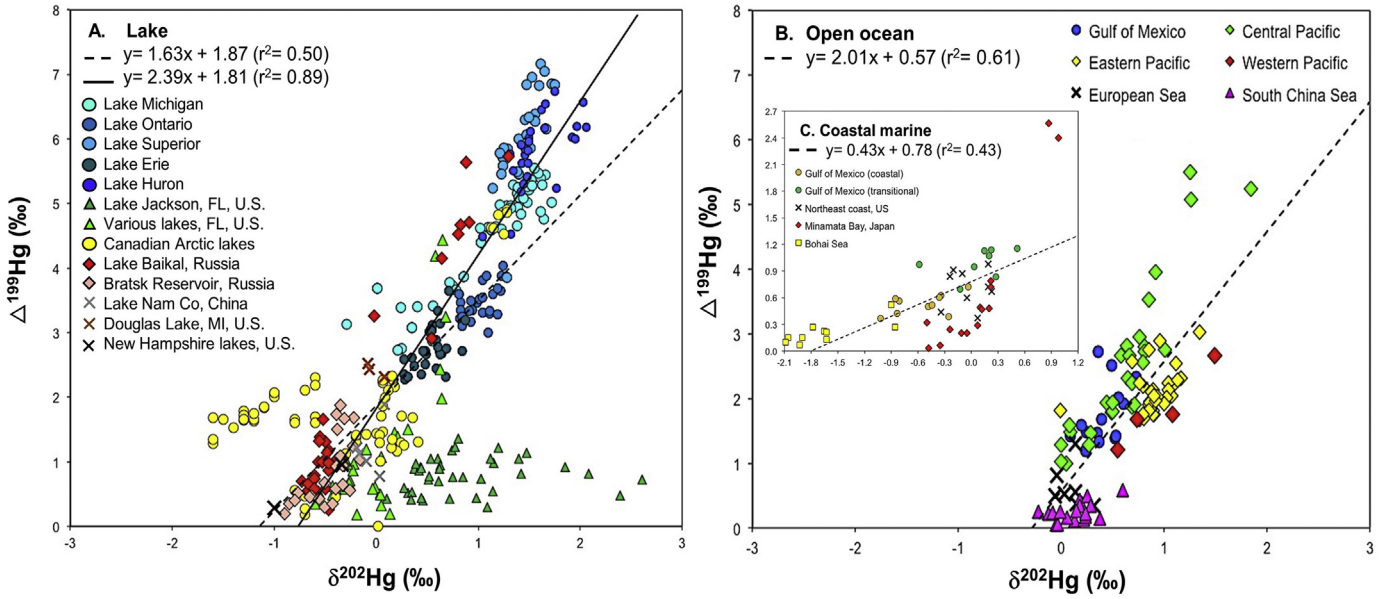

Fig. 9. δ^{202}Hg and Δ^{199}Hg values of lake (A), open ocean (B), and coastal marine fish (C). The dotted lines represent the overall regression. The solid line represents the regression excluding a few outlier sites (see Section 3.4.1.). All regressions are statistically significant ($p < 0.05$).

3.4. Fish

3.4.1. MMHg photodegradation (Δ^{199}Hg)

Fish collected from various lake, coastal, and open ocean environments display a wide range in δ^{202}Hg (-2.09 to 2.61‰) and a particularly wide range in Δ^{199}Hg (0.00 to 7.16‰; Fig. 9). The elevated Δ^{199}Hg in fish has been attributed to the trophic transfer of MMHg that has undergone significant photodegradation in the environment prior to bioaccumulation (e.g., Bergquist and Blum, 2007; Kwon et al., 2012, 2013). Both freshwater and marine fish often show correlated increases in δ^{202}Hg and Δ^{199}Hg (Fig. 9), consistent with experimental studies that report increasing δ^{202}Hg and Δ^{199}Hg in remaining IHg and MMHg during IHg photoreduction and MMHg photodegradation (Bergquist and Blum, 2007). In fact, with the exception of fish from only a few specific lakes (Lake Jackson, Florida, U.S.A. and a few Canadian Arctic lakes; Fig. 9A), most lake fish follow the experimental slope produced by varying degrees of MMHg photodegradation ($y = 2.43x + 0.75$ at 1mg/L DOC; Bergquist and Blum, 2007). This suggests that lake fish are exposed to MMHg that has undergone a similar photodegradation mechanism as occurs in laboratory experiments (mediated by DOC). Marine coastal and open-ocean fish, on the other hand, display significantly lower Δ^{199}Hg/δ^{202}Hg slopes compared to lake fish (Fig. 9B, C). This is due to either active microbial demethylation of MMHg in the oceanic water column resulting in a higher δ^{202}Hg in the remaining MMHg, or differences in DOC levels and/or ligands facilitating MMHg photodegradation between freshwater and marine systems (Motta et al., 2019).

Blum et al. (2013) observed a consistent Δ^{199}Hg/δ^{202}Hg slope between fish collected from the central Pacific Ocean and the experimental slope from MMHg photodegradation with natural DOC (Bergquist and Blum, 2007). In that study, the measurable δ^{202}Hg deviation between a few fish species and the experimental slope was explained by microbial methylation and microbial demethylation in the oceanic water column. The differences in the predominant ligands, consisting of various functional groups in dissolved organic matter (DOM), may also explain the lower Δ^{199}Hg/δ^{202}Hg slope in the open ocean fish compared the freshwater fish. Similar to Δ^{199}Hg/δ^{202}Hg, the open ocean and coastal marine fish displayed lower Δ^{199}Hg/Δ^{201}Hg slopes (open ocean ~1.21; coastal marine ~1.18) compared to lake fish (~1.26). Zheng and Hintelmann (2010a) observed a slower IHg photoreduction in the presence of ligands with sulfur-containing functional groups (thiol, disulfide/disulfane, thioether) compared to those without reduced sulfur groups (oxygen/nitrogen donor groups such as carboxylic, phenol, amine groups). Mercury typically displays a stronger binding affinity towards reduced sulfur-containing functional groups (Ravichandran, 2004). Binding of mercury to oxygen-functional groups, which are present at high abundances in freshwater, is thought to occur under high mercury to DOC ratios (~10 ug Hg/mg of DOM; Haitzer et al., 2002). It may be possible that, while most mercury in the open ocean is bound to reduced sulfur-containing functional groups, some mercury (which occurs at a higher concentration in freshwater) may be bound to oxygen/nitrogen donor groups, resulting in higher Δ^{199}Hg/δ^{202}Hg and Δ^{199}Hg/Δ^{201}Hg slopes. Chandan et al. (2014) also observed significantly different Δ^{199}Hg/Δ^{201}Hg slopes between experiments (MMHg photodegradation ~1.4) and natural freshwater fish. The authors attributed this to either the differences in the ligands bound to MMHg during natural versus experimental photodegradation or mixtures of MMHg photodegradation and IHg photoreduction from natural freshwater. We note that these conclusions are speculative and further experimental and field studies are required to explain the subtle Δ^{199}Hg/Δ^{201}Hg and Δ^{199}Hg/δ^{202}Hg differences between lake and open-ocean fish.

Given that photodegradation is important as a net MMHg sink in aquatic ecosystems, Δ^{199}Hg of fish has been useful for estimating the degree (%) of MMHg photodegradation prior to ecosystem exposure (e.g., Balogh et al., 2015; Blum et al., 2013; Gehrke et al., 2011b; Lepak et al., 2018; Kwon et al., 2013, 2014, 2015; Senn et al., 2010; Sherman and Blum, 2013). Despite our large dataset, the estimated % MMHg photodegradation are only meaningful on an ecosystem level or across ecosystems when fish species with similar life history characteristics are compared. The study by Blum et al. (2013) is an example for the former case. This study estimated a vertical difference in % MMHg photodegradation using Δ^{199}Hg of fish that feed at varying depths within the central Pacific Ocean. In regards to comparing fish species with similar life history characteristics, Sherman and Blum (2013) estimated % MMHg photodegradation across 11 lakes in Florida, U.S.A. using Δ^{199}Hg of a single fish species (largemouth bass) with similar size (> 178 mm in length). The authors observed 4 to 40% MMHg photodegradation across the lakes, which correlated significantly with the water turbidity as measured using secchi depth. We suggest that the

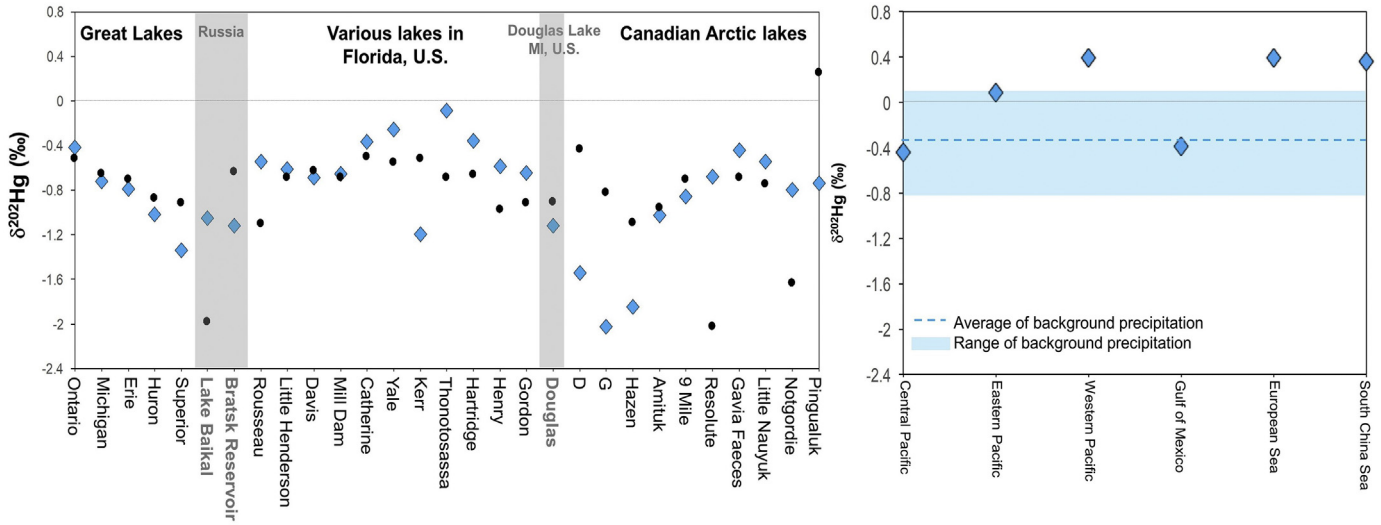

Fig. 10. The estimated δ^{202}Hg for MMHg using fish (blue diamonds) and average δ^{202}Hg of sediment (black circle) from lakes (A), and open ocean (B).

characterization of fish life histories needs to be completed before performing ecosystem-wide comparisons of the net MMHg sink caused by photodegradation using fish Δ^{199}Hg. Further experimental studies on photoreduction and photodegradation of various mercury species and those bound to environmentally relevant ligands are also necessary to interpret the mechanisms driving the Δ^{199}Hg/Δ^{201}Hg differences observed between freshwater and marine fish.

3.4.2. Site of MMHg production (δ^{202}Hg)

MMHg is thought to be produced biotically in bottom waters and/or surface sediment of lakes, wetlands, rivers, and coastal systems (Benoit et al., 2003; Gilmour and Henry, 1991; Ullrich et al., 2001) and in the open ocean water column (Blum et al., 2013; Eckley and Hintelmann, 2006; Sunderland et al., 2009). Previous studies have established δ^{202}Hg linkages between sediment (IHg) and fish (MMHg) in order to evaluate the location of MMHg production in several freshwater systems (Kwon et al., 2014, 2015; Tsui et al., 2012, 2014). Assuming that fish with the highest Δ^{199}Hg contain mercury that is mainly in the form of MMHg (~100% MMHg) and by applying the experimental slope of Δ^{199}Hg/δ^{202}Hg for photodegradation (Bergquist and Blum, 2007) we have estimated δ^{202}Hg for MMHg prior to photodegradation (Fig. 10A). For studies that report sediment δ^{202}Hg, we find that the estimated MMHg δ^{202}Hg values are similar to the average δ^{202}Hg of their respective sediment (average $\delta^{202}Hg_{estimated\ MMHg}$-$\delta^{202}Hg_{sediment}$ = 0.02‰, range = -1.2 to 1.35‰), confirming that sediment is an important site for MMHg production in many freshwater ecosystems. Some exceptions are observed in Canadian Arctic lakes (D, G, Resolute) and in Russian lakes (Lake Baikal and Bratsk Reservoir), which exhibit larger than ~0.9‰ differences in δ^{202}Hg between the sediment and the estimated MMHg (Fig. 10A). It is possible that fish from certain lakes may be exposed to MMHg derived externally and delivered via terrestrial runoff, and that this MMHg is characterized by highly negative δ^{202}Hg that is similar to foliage and soil (Fig. 6). This is also consistent with previous studies from Douglas Lake in Michigan (Kwon et al., 2015) as well as others that have illustrated the importance of runoff from wetlands and permafrost as a source of MMHg to some Arctic lakes (Loseto et al., 2004; Pérez-Rodríguez et al., 2019).

In the open ocean (Fig. 10B) the estimated MMHg δ^{202}Hg values (-0.44 to 0.39‰) prior to photodegradation are generally higher compared to freshwater (-2.03 to -0.09‰) and are similar to the range for background precipitation (-0.80 to 0.13‰; Fig. 3A). This is consistent with Blum et al. (2013) and Motta et al. (2019), who suggested that mercury deposited via wet deposition is likely methylated in the water column, which is then photochemically degraded at varying water depths (upper 200m) prior to uptake. While oceanic sediment may be an important site for mercury methylation, transport of MMHg from marine sediment to the near-surface is likely limited due to the water depth and limited linkages between benthic-pelagic food webs.

3.4.3. Sources that become bioavailable (Δ^{200}Hg, Δ^{204}Hg)

In the context of the MC, the ability to precisely identify bioavailable mercury sources subject to methylation and bioaccumulation are important in addition to the biogeochemical processes affecting mercury that were discussed in the sections above. An increasing number of studies have reported that fish Δ^{200}Hg values can be helpful for identifying sites of MMHg production and sources subject to methylation prior to ecosystem exposure (e.g., Lepak et al., 2018). Our compilation of fish Δ^{200}Hg and Δ^{204}Hg (Fig. 11) also illustrates that these values can aid in interpretation of the observed δ^{202}Hg differences between MMHg and sediment (Fig. 10). There is a relatively wide Δ^{200}Hg variation across lakes, with largemouth bass from 11 lakes in Florida, U.S.A. showing particularly elevated Δ^{200}Hg (Fig. 11A). In that study, Sherman and Blum (2013) also observed elevated sediment Δ^{200}Hg (average 0.11, range 0.04 to 0.18) and small δ^{202}Hg differences between the estimated MMHg (from largemouth bass) and sediment. The authors suggested that atmospherically deposited mercury via wet deposition was sorbed to particles and deposited to the sediment prior to being methylated and bioaccumulated into food webs. In another study, Lepak et al. (2018) observed larger than ~1‰ differences in δ^{202}Hg between pelagic fish (walleye and trout) and bulk sediments in the Great Lakes. Elevated Δ^{200}Hg values were also observed in pelagic fish (but not in sediments) consistent with those measured in precipitation, suggesting that mercury derived via wet deposition is methylated in the water column rather than in the sediment prior to bioaccumulation. We note that this is in contrast with the observed small δ^{202}Hg differences between the estimated MMHg (using pelagic fish) and sediment (Fig. 10A) from the Great Lakes region. This suggests that the interpretation of δ^{202}Hg alone may provide misleading information regarding mercury sources subject to methylation and bioaccumulation.

Among only a few studies that have reported both Δ^{200}Hg and Δ^{204}Hg of fish, we observed a negative linear relationship between Δ^{200}Hg and Δ^{204}Hg and a Δ^{200}Hg/Δ^{204}Hg slope of -0.33 (r^2 = 0.40, $p < 0.05$; Fig. 11B), similar to precipitation (-0.2; Fig. 3B). While this is speculative, the spatial differences in fish Δ^{200}Hg and Δ^{204}Hg may suggest that the relative input and/or bioavailability of precipitation may differ by site. For instance, positive Δ^{200}Hg and negative Δ^{204}Hg were more pronounced at locations with a larger average annual precipitation such as Florida (~1500mm) and the Central Pacific Ocean

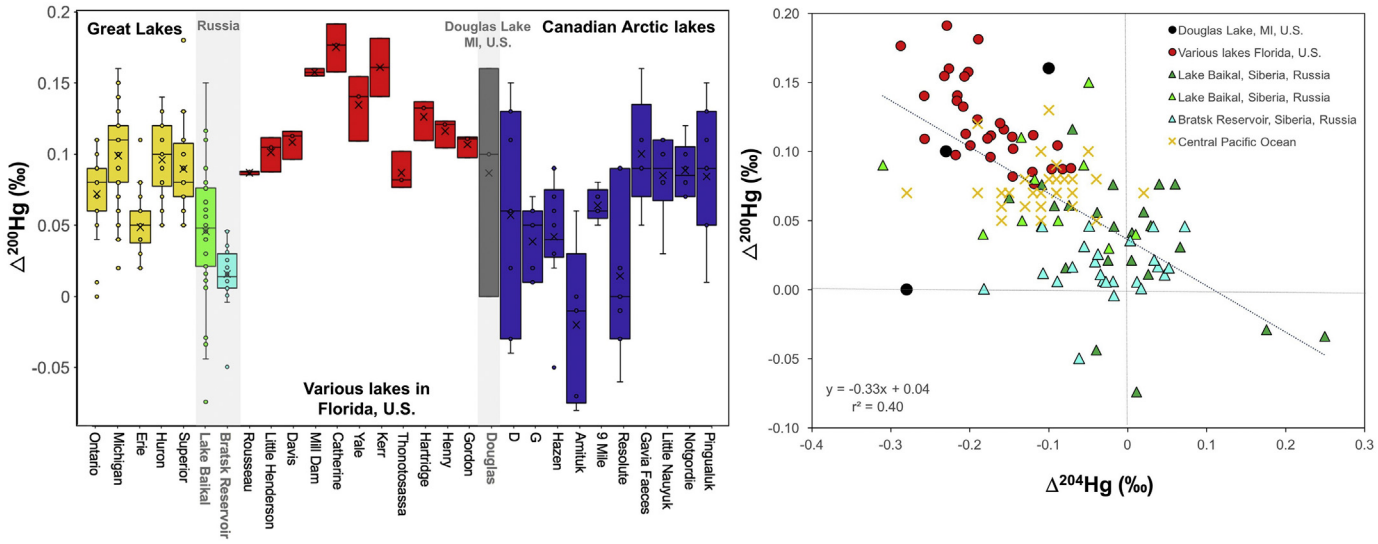

Fig. 11. Δ^{200}Hg values (A), and Δ^{204}Hg and Δ^{200}Hg values of fish (B) reported from various locations. The dotted line represents a regression between Δ^{204}Hg and Δ^{200}Hg of fish. The regression is statistically significant ($p < 0.05$).

(~2600mm) compared to Lake Baikal, Russia (300-400mm). In Florida (Sherman and Blum, 2013) and the Central Pacific Ocean (Blum et al., 2013), it was also found that mercury recently deposited via precipitation is a more important mercury source subject to methylation and bioaccumulation compared to mercury that pre-existed in sediments. The differences in fish species as well as their life history characteristics such as trophic position, feeding behavior, and feeding depth may also explain the observed variation of Δ^{200}Hg and Δ^{204}Hg both within and between sites. We suggest that further studies that characterize Δ^{200}Hg and Δ^{204}Hg in various environmental compartments of sediments and precipitation as well as in fish species of similar feeding behavior along environmental gradients are needed to evaluate the prospects and limitations of using Δ^{200}Hg and Δ^{204}Hg for the MC.

4. Implications for the global monitoring program

In this section we summarize the areas of uncertainty and potential applicability of mercury isotope measurements for the GMP. The ability to observe changes in mercury sources across a large spatial scale using mercury isotope values is expected to aid in a global comparison and to be useful as one component of the GMP. The process information is also important for establishing environmental baselines necessary for understanding the present and better predicting future ecosystem responses to a widespread upstream regulation of mercury under the MC. For each ecosystem and environmental sample type discussed above, Table 1 addresses a series of specific questions focused on determining the applicability for the GMP and EE. Specifically we address: 1) at what level can mercury ***sources*** be distinguished, 2) what types of biogeochemical ***processes*** are particularly relevant for establishing environmental baselines, and 3) at what ***spatial scale*** can we observe differences and/or changes in mercury sources and processes?

The measurements of mercury isotope ratios in TGM appear to be the most direct and effective way of utilizing mercury isotopes as part of the GMP. The linear regression between δ^{202}Hg and Δ^{199}Hg of TGM collected from urban-industrial and background sites (Fig. 2A) indicates that TGM isotopic compositions provide a clear distinction between anthropogenic and background sources of atmospheric mercury across a large spatial scale. Establishing spatiotemporal trends in TGM isotopic compositions via existing monitoring networks are expected to provide information regarding spatially and temporally variable changes in anthropogenic mercury contributions to the atmosphere under the MC implementation. An increasing number of research groups are also developing automated systems for sampling of atmospheric Hg^0 for mercury isotope measurements (e.g., Jiskra et al., 2019). Given the uncertainty in interpreting the observed trends in atmospheric Hg^0 concentrations (Slemr et al., 2011; Soerensen et al., 2012; Zhang et al., 2016), we suggest that the records of TGM isotopic compositions could become a valuable tool for diagnosing mercury sources responsible for changes under the MC.

Except for precipitation samples impacted by CFPP, our compilation study did not show a clear isotopic distinction between precipitation collected from urban and background sites (Fig. 3A). The Δ^{200}Hg and Δ^{204}Hg values of precipitation; however, exhibited spatial patterns, possibly caused by varying extents of atmospheric oxidation of Hg^0 (Fig. 3B). The MC emphasizes the need to generate globally comparable results not only on the sources but also on the processes affecting mercury speciation. In this regard, the records of Δ^{200}Hg and Δ^{204}Hg in precipitation can generate spatially comparable process information governing atmospheric mercury fate via wet deposition. Moreover, Δ^{200}Hg and Δ^{204}Hg can be used to differentiate between natural and other policy-driven changes in atmospheric mercury levels, transformations, and the extent of deposition. Recent observations suggest that tropospheric bromine, a strong mercury oxidant, has been decreasing at a rate of 0.1-0.15 ppt/year since its peak in 1998 due to the Montreal Protocol on Substances that Deplete the Ozone Layer (Montzka et al., 2011). Reduction in the tropospheric bromine compositions driven by other environmental policies may reduce the oxidation capacity of atmospheric Hg^0 and decrease the magnitude of mercury deposition. With the consideration of subtle Δ^{200}Hg and Δ^{204}Hg anomalies, we suggest that the understanding of spatially variable atmospheric processes would aid the interpretation of the observed mercury wet deposition concentration trends (e.g., Butler et al., 2008; Weiss-Penzias et al., 2016) under the MC.

In forest ecosystems, foliage and litter samples can be used to distinguish between anthropogenic and background atmospheric mercury sources over both short-term (growing season; Yuan et al., 2019) and longer-term periods (Wang et al., 2016; Yu et al., 2016). The rapid turnover (Yuan et al., 2019) and absence of significant MIF_{even} during foliage uptake of atmospheric Hg^0 suggests that Δ^{199}Hg in conjunction with Δ^{200}Hg may effectively trace relative changes in anthropogenic mercury influences, particularly in regions where atmospheric mercury monitoring networks do not exist. Many recent discoveries have been made regarding the importance of forest ecosystems as a global sink for atmospheric Hg^0. Increasing land use change via deforestation could

Table 1
Types of mercury sources and processes that can be distinguished for the GMP and EE and the associated uncertainties and future research needs for using mercury isotope ratios of each environmental sample. The spatial scale in which the differences or changes in mercury sources and processes can be observed is also given.

	Sources	Process	Spatial	EE vs GMP	Uncertainties/needs
Atmosphere					
TGM	Anthropogenic vs background	–	Regional-global	GMP	Distinguishing legacy mercury sources
Precipitation	Coal-fired power plant	Atmospheric oxidation, reduction	Regional-global	GMP	Other atmospheric processes leading to MDF, MIF_{odd}
PBM	Seasonal air mass transport	Atmospheric oxidation, reduction	Local-regional	EE	Need to couple backward trajectories of air masses, limited to local scale
Terrestrial					
Foliage, fresh litter	Anthropogenic vs background	–	Regional-global	GMP	Require a broader spatial scale evaluation
Forest floor	Precipitation vs soil vs foliage	Land use changes	Regional-global	GMP	MDF, MIF_{odd} compromising source signature
Soil	Anthropogenic vs background	Climatic influences on Hg^0 uptake via foliage	Regional-global	–	Vegetative cover driving the differences in mercury isotope ratios
Aquatic					
Sediment	Types of anthropogenic sources	–	Local-regional	EE	Biogeochemical processes compromising source signature
Fish	Bioavailable source	Methylation site, photo-degradation	Local-regional	EE	Constraining fish species with similar life history characteristics

lead to a lower Hg^0 contribution via litterfall and higher Hg^{2+} and Hg_P contributions via wet and dry deposition to forest ecosystems. We suggest that such human activities can be monitored more accurately via the monitoring of mercury isotope ratios in forest samples such as forest floor and mineral soil rather than via only concentration analyses.

The major difference between the samples discussed thus far and the analysis of sediment and fish is that while mercury isotope ratios of TGM, precipitation, foliage, and litter dominantly reflect the atmospheric mercury species (Hg^0 and Hg^{2+}), sediment and fish represent mixtures of multiple mercury species (IHg, MMHg) and input pathways (atmospheric deposition, anthropogenic releases, terrestrial runoff) that have been integrated over time and have undergone numerous biogeochemical fractionation processes. It is likely that the sediment samples collected for the GMP that are broadly characterized as “non-point source influenced" actually reflect mixtures of multiple mercury sources and input pathways. The observed wide ranges in mercury isotope ratios of non-point source influenced sediments (Fig. 7) suggest that the interpretation of globally comparable source, process, and fate information using sediment mercury isotope ratios will be difficult. In regards to fish, generating comparable information on mercury source and processes such as the extent of MMHg photodegradation (Fig. 9) and input of atmospheric mercury via $\Delta^{200}Hg$ and $\Delta^{204}Hg$ (Fig. 11) will require standardization of measurements on consistent fish species with similar life history characteristics. Moreover, given that the methodological approaches used to interpret the sites of MMHg production ($\delta^{202}Hg$ difference between sediment and estimated MMHg; Fig 10) can lead to misleading conclusions, site-specific information including $\Delta^{200}Hg$ and $\Delta^{204}Hg$ needs to be actively employed to identify the sites of MMHg production and the sources of mercury subject to methylation.

5. Implications for the effectiveness evaluation

This review shows that mercury isotope ratios provide a promising measurement tool for determining sources of mercury subject to regulation and for generating large scale patterns of changes in mercury sources, processes, and fate. Nevertheless, a number of limitations still exist in the widespread utilization of mercury isotopes for the MC. The major limitation arises from the MC’s current scope of the EE, which is to utilize globally comparable results on mercury sources, processes, and fate to establish trends. The current scope leads to a number of questions regarding the EE: “Shouldn’t the EE’s scope be in parallel with the goal of the MC of mitigating ecosystem and human health impacts from mercury exposure?” and “what type of scientific information should be gathered to predict the MC’s effectiveness and to generate resource-effective targets for the EE?”

We suggest that evidence of the effects of source regulation needs to be gathered from a range of health-relevant locations and media spanning remote regions (where insights into the global health may be gained) and local point source regions (where most human health risks are raised) to maximize the effectiveness of the MC. While the former may be achieved by generating temporal trends from the GMP data, the assessment of the latter is not included in the MC. Such objectives pose risks of excluding a number of countries that do not have the capability to establish GMP and that are undergoing rapid economic and industrial development, leading to mercury pollution. Moreover, given that many local point source regions represent mercury hotspots and public health concerns, the effectiveness of the proposed regulation and mercury abatement activities should be evaluated swiftly to identify additional remedial, management, and/or technological issues. The EE of the Stockholm Convention on Persistent Organic Pollutants (POPs; Article 16) is a good example, and emphasizes the need to eliminate or reduce the releases from intentional and unintentional production and uses or releases from stockpiles and wastes. It also points to the importance of evaluating whether environmental pollutant levels are

decreasing over time on a local scale (UN Environment, 2017b).

By establishing an additional scope that is aligned specifically with the MC's goal, we suggest that the utilization of mercury isotopes can be further expanded to address the challenges of the MC. For instance, at locations proximal to local mercury point sources, many ecosystem and public health concerns are initiated from the deposition of anthropogenically emitted mercury and releases from activities that use or produce mercury. Previous studies have shown that mercury emissions from local point source activities can accumulate substantially in soil and aquatic media and result in elevated mercury concentrations in fish and rice, leading to public health concerns (e.g., Li et al., 2009; Kwon et al., 2018). Some anthropogenic activities such as biomass burning for residential heating and agricultural practices are not governed under the MC, but still represent important mercury emission sources in a number of developing countries (Huang et al., 2018). In this regard, the measurements of Hg_P isotope ratios may provide a means of assessing the effectiveness of local to regional scale regulations on anthropogenic mercury emissions and for re-evaluating domestically important anthropogenic activities responsible for ecosystem and human health impacts (Table 1). The studies by Huang et al. (2016, 2018) demonstrate that we may be able to distinguish between seasonally relevant local atmospheric mercury sources (i.e., coal combustion, biomass burning) at urban-industrial locations (Fig. 4). It is important, however, to emphasize that the measurements of Hg_P isotopic compositions alone may be insufficient for source appointment. We urge that the full utility of Hg_P isotopic compositions for local point mercury source identification needs to be explored further at locations other than China and India and by coupling of backward trajectories of air masses and characterizing source materials (i.e., local coal and biomass used for heating).

In regards to the sources that release mercury into aquatic ecosystems, the measurements of sediment mercury isotope ratios can aid the identification of sources, and pathways leading to mercury hotspots. This is also in line with the MC's Article 12 on mercury contaminated sites, which emphasizes the need to discover new approaches for contaminated site identification and characterization. As illustrated in Fig. 8, we observed relatively distinct mercury isotope ratios in the sediments impacted by various mercury point source activities, indicating that the identification of mercury point sources and activities may be possible via the measurement of mercury isotope ratios at local contaminated sites. Moreover, while many countries have already phased out anthropogenic activities causing severe mercury pollution (i.e., chlor-alkali production, mercury-added products, ASGM), a number of countries still have ongoing illegal ASGM activities. A recent study by Adler Miserendino et al. (2018) measured mercury isotope ratios of sediments and soils near ASGM sites in Brazil and found that increased soil erosion associated with land-cover and land-use change contributed to elevated mercury concentrations downstream of ASGM activities. Such information is critical for seeking strategies to mitigate land-use changes in addition to direct ASGM activities.

Consumption of fish is directly linked to public health risks via mercury exposure even in remote regions without significant point sources of mercury. We propose preliminary assessments to identify aquatic ecosystems and fish species that are sensitive to atmospheric mercury deposition relative to other mercury sources such as point source releases and terrestrial runoff. This will provide a more targeted and resource-effective EE (Table 1). Specifically, the $\Delta^{200}Hg$ and $\Delta^{204}Hg$ of fish as well as the degree of $\delta^{202}Hg$ offset between sediment and estimated MMHg may be used as a quick screening procedure to predict potential responses of fish under the widespread upstream regulation of anthropogenic mercury emissions via the MC. We found that the small $\delta^{202}Hg$ difference between sediment and MMHg (Fig. 10A) as well as negative $\Delta^{200}Hg$ and positive $\Delta^{204}Hg$ in fish (Fig. 11A) are consistent with sediment as the dominant MMHg production site. In contrast, the large $\delta^{202}Hg$ difference between sediment and MMHg (Fig. 10B), as well as positive and negative fish $\Delta^{200}Hg$ and $\Delta^{204}Hg$, respectively (Fig. 11B) (as in the case of the open ocean and the Great Lakes) may indicate that atmospherically deposited mercury is converted to MMHg in the water column prior to ecosystem exposure. The study by Sherman and Blum, 2013 also provides an interesting case study in which mercury deposited from the atmosphere to sediment and that has then undergone methylation, was found to be the dominant mercury source to largemouth bass in Florida lakes (see Section 3.4.3). Perhaps the observation of more rapid changes in fish mercury concentration and isotope values may be achieved in waterbodies such as the Great Lakes, given the rapid turnover of mercury in the water column compared to sediments. As such, we suggest that the evaluation of ecosystems and fish species to find those most sensitive to atmospheric mercury deposition will allow more targeted EE as well as future predictions of the MC.

6. Conclusions

This literature review suggests that the measurements of mercury isotope ratios in various environmental samples and ecosystems can help address the challenges of the GMP and the EE of the MC. In regards to the GMP, we found that the measurements of atmospheric samples such as TGM and precipitation provide the most direct way of generating comparable information on sources, processes, and fate of atmospheric mercury. Samples of foliage and litter are dominantly influenced by atmospheric Hg^0 and displayed distinct mercury isotope ratios consistent with either background or anthropogenic sources. In contrast to these samples, the utilization of sediment and fish for the GMP appear difficult given that they represent mixtures of multiple mercury sources and are influenced by complex processes leading to mercury isotope fractionation.

A vast number of studies concerning the measurements of mercury isotope ratios have been conducted primarily at local scales to understand the sources, processes, and fate of mercury in specific environmental reservoirs. By proposing an additional objective for the EE that is aligned specifically with the goal of the MC, we suggest that the utility of mercury isotopes can be further expanded to local mercury hotspots and media that are directly relevant for human health. Specifically, the measurements of atmospheric Hg_P and sediment mercury isotope ratios at locations of point source mercury emissions and releases, respectively, can be used to evaluate the effectiveness of local scale regulations and for re-evaluating domestically important mercury emissions sources, which are not governed under the MC (i.e., biomass burning). Humans are primarily exposed to mercury via fish consumption and we suggest that using mercury isotopes to screen ecosystems and fish species that are sensitive to atmospheric deposition can allow both accurate prediction and a resource-effective target for EE. Young-of-the-year fish that have limited spatial movement and feed primarily on plankton from the water column may also be an effective bio-sentinel(s) for evaluating the effectiveness of the MC.

A number of challenges still remain in regards to the widespread utility of mercury isotope measurements for the MC. A major pitfall of using mercury isotope ratios for source apportionment is the overlapping of source signatures and complex biogeochemical processes leading to isotopic fractionation in environmental reservoirs. While a number of studies have utilized statistical methods (e.g., Janssen et al., 2019), isotopic mixing models, (e.g., Bartov et al., 2013) and separation of mercury species (e.g., Brocza et al., 2019) to better decipher the differences in source signatures, the interpretation of low-level speciation and biogeochemical processes are limited. Additional effort is needed to understand mercury isotope fractionation pathways during diverse biogeochemical processes. In addition, whole ecosystem studies in which various environmental samples (i.e., sediments, precipitation, fish) are measured simultaneously within an ecosystem are necessary for identifying additional processes leading to mercury isotope fractionation and pathways of mercury input. This information will ultimately serve as an important baseline prior to the MC implementation.

In the context of using mercury isotopes for deciphering signals due to policy changes versus natural variations, one of the major obstacles is the need for identification of legacy mercury sources (mercury that has been recycled through the environment from previous anthropogenic emissions). With widespread upstream regulation of anthropogenic mercury emissions, we expect the proportion of legacy mercury sources to increase in various environmental reservoirs relative to "new" anthropogenic sources (Kwon and Selin, 2016). Other environmental forcing such as climate change may also increase the magnitude of legacy mercury re-emission into the atmosphere. With such information, we can establish more precise environmental baselines and explain observed subtle differences in mercury isotope ratios between environmental samples and ecosystems.

Declaration of Competing Interest

None.

Acknowledgments

This work was supported by the National Institute of Environment Research (NIER) funded by the Ministry of Environment (MOE) of the Republic of Korea (NIER-2019-01-01-079), the National Research Foundation of Korea (NRF) funded by the Korea government (MSIT) (NRF-2019R1F1A1058928), the research program of the Korean Institute of Ocean Science and Technology (PE99883), and the POSTECH Basic Science Research Institute Grant. The data used to plot fig.s can be found at https://github.com/saeyunk/isotope_data (DOI 10.5281/zenodo.8475).

Appendix

Table A.1
List of sample types, sampling location, sample number and the associated references used for the data compilation.

Sample type (Fig. #)	Sampling location	Number of samples	Reference
Atmosphere			
TGM (Fig. 2A, 2B)	Surface evasion: Grand Bay, Mississippi, U.S.A.	13	Rolison et al., 2013
	Surface evasion: Guizhou, China	2	Yin et al., 2013a
	Background: Alaska, U.S.A.	2	Sherman et al., 2010
	Background: Wisconsin, U.S.A.	3	Demers et al., 2013
	Background & urban-industrial: Midwest, U.S.A.	7	Gratz et al., 2010
	High altitude mountain & urban-industrial: Mountrain Ailao, Yunnan, Mountain Damei, Zhejiang, Beijing, and Guizhou, China	102	Yu et al., 2016
	High altitude mountain: Pic du Midi Observatory, France	27	Fu et al., 2016
	Urban-industrial: Shaanxi, China	21	Xu et al., 2017
Precipitation (Fig. 3A)	CFPP: Xiamen, China	18	Huang et al., 2018
	CFPP: Florida, U.S.A.	41	Sherman et al., 2012
	Urban & background: Midwest, U.S.A.	40	Sherman et al., 2015b
	Urban & semirural & background: Midwest, U.S.A.	20	Gratz et al., 2010
	Urban: Guiyang, China	15	Wang et al., 2016
	Semirural: Peterborough, Ontario, Canada	19	Chen et al., 2012
	Semirural: San Francisco Bay, California, U.S.A.	3	Donovan et al., 2013
	Background: Wisconsin, U.S.A.	5	Demers et al., 2013
	Background: Tibetan Plateau, China	4	Yuan et al., 2015
	Ocean: Shipboard and Hawaii, U.S.A.	8	Motta et al., 2019
Precipitation (Fig. 3B)	CFPP: Florida, U.S.A.	41	Sherman et al., 2012
	Semirural: San Francisco Bay, California, U.S.A.	3	Donovan et al., 2013
	Background: Wisconsin, U.S.A.	5	Demers et al., 2013
	Background: Michigan, U.S.A.	6	Sherman et al., 2015b
	Background: Vermont, U.S.A.	6	Sherman et al., 2015b
	Ocean: Shipboard and Hawaii, U.S.A.	8	Motta et al., 2019
	Semirural: Florida, U.S.A.	15	Sherman et al., 2012
	Urban: Ohio, U.S.A.	16	Sherman et al., 2015b
	Urban: Michigan, U.S.A.	12	Sherman et al., 2015b
PM2.5 (Fig. 4A)	Beijing, China	23	Huang et al., 2016
PM10 (Fig. 4A)	Kolkata, Inida	52	Das et al., 2016
Total PBM (Fig. 4B)	Xiamen, China	38	Huang et al., 2018
	Shaanxi, China	67	Xu et al., 2017
	Guiyang, China	46	Yu et al., 2016
	Zhejiang, China		
Terrestrial			
Foliage (Fig. 6A)	Wisconsin, U.S.A.	18	Demers et al., 2013
	Various locations in the U.S.A.	9	Zheng et al., 2016
Litter (Fig. 6A)	Chinese litter	99	Yu et al., 2016 Wang et al., 2016
	Various locations in the U.S.A.	7	Zheng et al., 2016
Forest floor (Fig. 6A)	Sierra Nevada, CA, U.S.A.	2	Tsui et al., 2012
	Pellston, MI, U.S.A.	1	Kwon et al., 2015
	Various locations in the U.S.A.	22	Zheng et al., 2016
Urban soil (Fig. 6B)	Northeast, France	14	Estrade et al., 2011
	Beijing, China	5	Huang et al., 2016
Mineral soil (Fig. 6B)	Wisconsin, U.S.A.	9	Demers et al., 2013
	Tibetan Plateau, China	18	Wang et al., 2016
	Various locations in the U.S.A.	38	Zheng et al., 2016

(*continued on next page*)

Table A.1 (*continued*)

Sample type (Fig. #)	Sampling location	Number of samples	Reference
Organic soil (Fig. 6B)	Michigan, U.S.A.	1	Kwon et al., 2015
	California, U.S.A.	1	Tsui et al., 2012
	Northern Sweden	15	Jiskra et al., 2017
	Various locations in the U.S.A.	8	Biswas et al., 2008
Sediment			
River			
Point source impacted (Fig. 7A, 7B)	Oakridge, Tennesee, U.S.A.	11	Bartov et al., 2013 Donovan et al., 2014
	Mill Creek, New Jersey, U.S.A.	3	Kwon et al., 2014
	South River, Virginia, U.S.A.	8	Washburn et al., 2017
	Puyango-Tumbes River, Educador	8	Schudel et al., 2018
	Idrijica River, Italy-Slovenia	3	Foucher and Hintelmann, 2009
	Gossan Creek, New Brunswick, Canada	18	Foucher and Hintelmann, 2006, Foucher et al., 2013
	Dashuixi River, Guizhou, China	20	Yin et al., 2013b, 2013c
	California Coast Range, U.S.A.	12	Donovan et al., 2016
	Almaden, Spain	6	Jiménez-Moreno et al., 2016
	New Idria, California	35	Smith et al., 2014
	Aveyron, France	22	Sonke et al., 2010
	Kempen, Belgium		
Non-point source influenced (Fig. 7A, 7B)	Aveyron, France	13	Sonke et al., 2010
	Kempen, Belgium		
	Oakridge, Tennesee, U.S.A.	35	Bartov et al., 2013 Donovan et al., 2014
	South River, Virginia, U.S.A.	5	Washburn et al., 2017
	Dashuixi River, Guizhou, China	2	Yin et al., 2013c
	Pearl River Delta, China	20	Liu et al., 2011
	Central Amazonian Basin	12	Araujo et al., 2018
Lake			
Point source impacted (Fig. 7A, 7B)	Baihua Reservoir, Guizhou, China	15	Feng et al., 2010
	Bratsk Reservoir, Siberia, Russia	9	Perrot et al., 2010
	Peruvian Andes, Educador	8	Cooke et al., 2013
	Almaden, Spain	8	Jiménez-Moreno et al., 2016
	Lake Ballinger, Washington, U.S.A.	10	Gray et al., 2013
	Manitoba, Canada	32	Ma et al., 2013
Non-point source influenced (Fig. 7A, 7B)	Peruvian Andes, Educador	7	Cooke et al., 2013
	Lake Wittington, Mississippi, U.S.A.	16	Gray et al., 2015
	Various locations in the U.S.A.	31	Das et al., 2015
	Various locations, Florida, U.S.A.	20	Sherman and Blum, 2013
	Lake Ballinger, Washington, U.S.A.	5	Gray et al., 2013
	Great Lakes region, U.S.A.	57	Lepak et al., 2015
	Various locations, Ontario, Canada	19	Chen et al., 2016
	Canadian Arctic lakes	19	Gantner et al., 2009
	Lake Baikal, Siberia, Russia	1	Perrot et al., 2010
	Hongfeng Reservoir, Guizhou, China	19	Feng et al., 2010
	Central Amazonian Basin	4	Araujo et al., 2018
	Esteras River, Alamden Spain	4	Jiménez-Moreno et al., 2016
	Puyango-Tumbes River, Educador	8	Schudel et al., 2018
	Manitoba, Canada	35	Ma et al., 2013
Pre-anthropogenic	Lake Ballinger, Washington, U.S.A.	4	Gray et al., 2013
(Fig. 7A, 7B)	Peruvian Andes, Educador	20	Cooke et al., 2013
Coastal/esutary			
Point source impacted (Fig. 7A, 7B)	Minamata Bay, Japan	18	Balogh et al., 2015 Foucher and Hintelmann, 2006
	San Francisco Bay, U.S.A.	2	Donovan et al., 2014
	Soča/Isonzo River estuary, Italy-Slovenia	6	Foucher and Hintelmann, 2009
	Paraiba do Sul River estuary, Brazil	11	Araujo et al., 2017
Non-point source influenced (Fig. 7A, 7B)	Northeast coast, U.S.A.	7	Kwon et al., 2014
	Gulf of Mexico, U.S.A.	4	Senn et al., 2010
	San Francisco Bay, U.S.A.	51	Gehrke et al., 2011b Donovan et al., 2014 Foucher and Hintelmann, 2006
	Cabretta Island, Florida, U.S.A.	41	Das et al., 2013
	Celestum Lagoon, Yucatan Penninsula, Mexico	5	Das et al., 2015
	Pearl River Delta, China	37	Yin et al., 2015
Pre-anthropogenic (Fig. 7A, 7B)	San Francisco Bay, U.S.A.	8	Donovan et al., 2014
Marine			
Point source impacted (Fig. 7A, 7B)	Norweign Sea	14	Rua-Ibarz et al., 2016
	Yasushiro Sea, Japan	12	Balogh et al., 2015
	Gulf of Trieste, Itlay-Slovenia	6	Foucher and Hintelmann, 2009
Non-point source influenced (Fig. 7A, 7B)	Campos Basin, Brazil	29	Araujo et al., 2017
	Gulf of Trieste, Itlay-Slovenia	7	Foucher and Hintelmann, 2009
	Central Portugese Margin	15	Mil-Homens et al., 2013
	Gulf of Mexico, U.S.A.	2	Senn et al., 2010
	South China Sea	6	Yin et al., 2015

(*continued on next page*)

Table A.1 (*continued*)

Sample type (Fig. #)	Sampling location	Number of samples	Reference
Pre-anthropogenic (Fig. 7A, 7B)	Mediterranean Sea	11	Gehrke et al., 2009
	Central Portugese Margin	6	Mil-Homens et al., 2013
Point source impacted sediment			
Fly ash (Fig. 8A)	Oakridge, Tennesee, U.S.A.	9	Bartov et al., 2013
Smelter (Fig. 8A)	Lake Ballinger, Mississippi, U.S.A.	10	Gray et al., 2013
	Manitoba, Canada	32	Ma et al., 2013
	Aveyron, France	22	Sonke et al., 2010
	Kempen, Belgium		
Chemical industries (Fig. 8A, 8B)	Minamata Bay, Japan	25	Balogh et al., 2015
	Guizhou, China	15	Feng et al., 2010
	South River, Virginia, U.S.A.	8	Washburn et al., 2017
	Bratsk Water Reservoir, Russia	9	Perrot et al., 2010
Metallic mercury (Fig. 8A, 8B)	Norweign Sea	14	Rua-Ibarz et al., 2016
	Oakridge, Tennesee, U.S.A.	2	Donovan et al., 2014
	Mill Creek, New Jersey, U.S.A.	3	Kwon et al., 2014
Mining (Fig. 8A, 8B)	New Idria, California	35	Smith et al., 2014
	Dashuixi River, Guizhou, China	8	Yin et al., 2013b
	Dashuixi River, Guizhou, China	12	Yin et al., 2013c
	Gossan Creek, New Brunswick, Canada	18	Foucher et al., 2013
	Idrijica River, Italy-Slovenia	15	Foucher and Hintelmann, 2009
	Puyango-Tumbes River, Ecuador		Schudel et al., 2018
	Almaden, Spain	14	Jiménez-Moreno et al., 2016
	Peruvian Andes, Educador	8	Cooke et al., 2013
	San Francisco Bay, U.S.A.	2	Donovan et al., 2013
	California Coast Range, U.S.A.	12	Donovan et al., 2016
Fish			
Lake (Fig. 9A, 10A, 11A)	Lake Michigan, U.S.A.	28	Bergquist and Blum, 2007
			Kwon et al., 2012
			Lepak et al., 2015
	Lake Ontario, U.S.A.	29	Lepak et al., 2015, 2018
	Lake Superior, U.S.A.	28	Lepak et al., 2015, 2018
	Lake Erie, U.S.A.	30	Lepak et al., 2018
	Lake Huron, U.S.A.	26	Lepak et al., 2018
	Lake Jackson, Florida, U.S.A.	40	Das et al., 2009
	Various lakes in Florida, U.S.A.	31	Sherman and Blum, 2013
	Canadian Arctic lakes	65	Gantner et al., 2009
	Lake Baikal, Siberia, Russia	34	Perrot et al., 2010, 2012
	Bratsk Reservoir, Siberia, Russia	24	Perrot et al., 2010
	Nam Co Lake, China	5	Liu et al., 2018
	Douglas Lake, Michigan, U.S.A.	3	Kwon et al., 2015
	New Hampshire lakes, U.S.A.	2	Bergquist and Blum, 2007
Open ocean (Fig. 9B, 10B, 11B)	Gulf of Mexico, U.S.A.	14	Senn et al., 2010
	Eastern Pacific	34	Madigan et al., 2018
	Central Pacific	28	Blum et al., 2013
	Western Pacific	18	Madigan et al., 2018
			Balogh et al., 2015
	European Sea	7	Cransveld et al., 2017
	South China Sea	18	Yin et al., 2016
Coastal (Fig. 9C)	Gulf of Mexico, U.S.A. (coastal)	10	Senn et al., 2010
	Gulf of Mexico, U.S.A. (transitional)	8	Senn et al., 2010
	Northeast coast, U.S.A.	9	Kwon et al., 2014
	Minamata Bay, Japan	12	Balogh et al., 2015
	Bohai Sea, China	10	Liu et al., 2018

References

Adler Miserendino, R., Guimarães, J.R.D., Schudel, G., Ghosh, S., Godoy, J.M., Silbergeld, E.K., Lees, P.S.J., Bergquist, B.A., 2018. Mercury pollution in Amapá, Brazil: Mercury amalgamation in artisanal and small-scale gold mining or land-cover and land-use changes? ACS Earth Space Chem 2, 441–450. https://doi.org/10.1021/acsearthspacechem.7b00089.

Araujo, B.F., Hintelmann, H., Dimock, B., Almeida, M.G., Rezende, C.E., 2017. Concentrations and isotope ratios of mercury in sediments from shelf and continental slope at Campos Basin near Rio de Janeiro, Brazil. Chemosphere 178, 42–50. https://doi.org/10.1016/j.chemosphere.2017.03.056.

Araujo, B.F., Hintelmann, H., Dimock, B., de Lima Sobrinho, R., Bernardes, M.C., de Almeida, M.G., Krusche, A.V., Rangel, T.P., Thompson, F., de Rezende, C.E., 2018. Mercury speciation and Hg stable isotope ratios in sediments from Amazon floodplain lakes—Brazil. Limnol. Oceanogr. 63, 1134–1145. https://doi.org/10.1002/lno.10758.

Balogh, S.J., Tsui, M.T.K., Blum, J.D., Matsuyama, A., Woerndle, G.E., Yano, S., Tada, A., 2015. Tracking the fate of mercury in the fish and bottom sediments of Minamata Bay, Japan, using stable mercury isotopes. Environ. Sci. Technol. 49 (9), 5399–5406. https://doi.org/10.1021/acs.est.5b00631.

Bartov, G., Deonarine, A., Johnson, T.M., Ruhl, L., Vengosh, A., Hsu-Kim, H., 2013. Environmental impacts of the Tennessee Valley Authority Kingston coal ash spill. 1. Source apportionment using mercury stable isotopes. Environ. Sci. Technol. 47 (4), 2092–2099. https://doi.org/10.1021/es303111p.

Benoit, J.M., Gilmour, C.C., Heyes, A., Mason, R.P., Miller, C.L., 2003. Geochemical and biological controls over methylmercury production and degradation in aquatic ecosystems. In: Cai, Y., Braids, O.C. (Eds.), Biogeochemistry of Environmentally Important Trace Elements. American Chemical Society.

Bergquist, B.A., Blum, J.D., 2007. Mass-dependent and mass-independent fractionation of Hg isotopes by photo-reduction in aquatic systems. Science 318, 417–420. https://doi.org/10.1126/science.1148050.

Biswas, A., Blum, J.D., Bergquist, B.A., Keeler, G.J., Xie, Z., 2008. Natural mercury isotope variation in coal deposits and organic soils. Environ. Sci. Technol. 42, 8303–8309. https://doi.org/10.1021/es801444b.

Blum, J.D., Bergquist, B.A., 2007. Reporting of variations in the natural isotopic composition of mercury. Anal. Bioanal. Chem. 388 (2), 353–359. https://doi.org/10.1007/s00216-007-1236-9.

Blum, J.D., Johnson, M.W., 2017. Recent developments in mercury stable isotope analysis. Rev. Mineral. Geochem. 82 (1), 733–757. https://doi.org/10.1515/

9783110545630-018.
Blum, J.D., Popp, B.N., Drazen, J.C., Choy, C.A., Johnson, M.W., 2013. Methylmercury production below the mixed layer in the North Pacific Ocean. Nat. Geosci. 6, 879. https://doi.org/10.1038/ngeo1918.
Blum, J.D., Sherman, L.S., Johnson, M.W., 2014. Mercury isotopes in earth and environmental sciences. Annu. Rev. Earth Planet. Sci. 42, 249–269. https://doi.org/10.1146/annurev-earth-050212-124107.
Brocza, F.M., Biester, H., Richard, J.H., Kraemer, S.M., Wiederhold, J.G., 2019. Mercury isotope fractionation in the subsurface of a Hg (II) chloride-contaminated industrial legacy site. Environ. Sci. Technol. 53, 7296–7305. https://doi.org/10.1021/acs.est.9b00619.
Buchachenko, A.L., 2001. Magnetic isotope effect: nuclear spin control of chemical reactions. J. Phys. Chem. A 105 (44), 9995–10011. https://doi.org/10.1021/jp011261d.
Butler, T.J., Cohen, M.D., Vermeylen, F.M., Likens, G.E., Schmeltz, D., Artz, R.S., 2008. Regional recipitation mercury trends in the eastern USA, 1998–2005: Declines in the Northeast and Midwest, no trend in the Southeast. Atmos. Environ. 42 (7), 1582–1592. https://doi.org/10.1016/j.atmosenv.2007.10.084.
Cai, H., Chen, J., 2016. Mass-independent fractionation of even mercury isotopes. Sci. Bull. 61 (2), 116–124. https://doi.org/10.1007/s11434-015-0968-8.
Chandan, P., Ghosh, S., Bergquist, B.A., 2014. Mercury isotope fractionation during aqueous photoreduction of monomethylmercury in the presence of dissolved organic matter. Environ. Sci. Technol. 49 (1), 259–267. https://doi.org/10.1021/es5034553.
Chen, J., Hintelmann, H., Feng, X., Dimock, B., 2012. Unusual fractionation of both odd and even mercury isotopes in precipitation from Peterborough, ON, Canada. Geochim. Cosmochim. Acta 90, 33–46. https://doi.org/10.1016/j.gca.2012.05.005.
Chen, H., Teng, Y., Lu, S., Wang, Y., Wang, J., 2015. Contamination features and health risk of soil heavy metals in China. Sci. Total Environ. 512, 143–153. https://doi.org/10.1016/j.scitotenv.2015.01.025.
Chen, J., Hintelmann, H., Zheng, W., Feng, X., Cai, H., Wang, Z., Yuan, S., Wang, Z., 2016. Isotopic evidence for distinct sources of mercury in lake waters and sediments. Chem. Geol. 426, 33–44. https://doi.org/10.1016/j.chemgeo.2016.01.030.
Cooke, C.A., Hintelmann, H., Ague, J.J., Burger, R., Biester, H., Sachs, J.P., Engstrom, D.R., 2013. Use and legacy of mercury in the Andes. Environ. Sci. Technol. 47, 4181–4188. https://doi.org/10.1021/es3048027.
Cransveld, A., Amouroux, D., Tessier, E., Koutrakis, E., Ozturk, A.A., Bettoso, N., Mieiro, C.L., Bérail, S., Barre, J.P.G., Sturaro, N., Schnitzler, J., Das, K., 2017. Mercury stable isotopes discriminate different populations of European seabass and trace potential Hg sources around Europe. Environ. Sci. Technol. 51 (21), 12219–12228. https://doi.org/10.1021/acs.est.7b01307.
Das, R., Salters, V.J., Odom, A.L., 2009. A case for in vivo mass-independent fractionation of mercury isotopes in fish. Geochem. Geophys. Geosyst. 10 (11). https://doi.org/10.1029/2009gc002617.
Das, R., Bizimis, M., Wilson, A.M., 2013. Tracing mercury seawater vs. atmospheric inputs in a pristine SE USA salt marsh system: mercury isotope evidence. Chem. Geol. 336, 50–61. https://doi.org/10.1016/j.chemgeo.2012.04.035.
Das, R., Landing, W., Bizimis, M., Odom, L., Caffrey, J., 2015. Mass independent fractionation of mercury isotopes as source tracers in sediments. Proced. Earth. Plan. Sci. 13, 151–157. https://doi.org/10.1016/j.proeps.2015.07.036.
Das, R., Wang, X., Khezri, B., Webster, R.D., Sikdar, P.K., Datta, S., 2016. Mercury isotopes of atmospheric particle bound mercury for source apportionment study in urban Kolkata, India. Elem. Sci. Anth. 4, 98. https://doi.org/10.12952/journal.elementa.000098.
Day, R.D., Roseneau, D.G., Berail, S., Hobson, K.A., Donard, O.F., Vander Pol, S.S., Pugh, R.S., Moors, A.J., Long, S.E., Becker, P.R., 2012. Mercury stable isotopes in seabird eggs reflect a gradient from terrestrial geogenic to oceanic mercury reservoirs. Environ. Sci. Technol. 46 (10), 5327–5335. https://doi.org/10.1021/es2047156.
Demers, J.D., Blum, J.D., Zak, D.R., 2013. Mercury isotopes in a forested ecosystem: implications for air-surface exchange dynamics and the global mercury cycle. Glob. Biogeochem. Cycles 27 (1), 222–238. https://doi.org/10.1002/gbc.20021.
Demers, J.D., Sherman, L.S., Blum, J.D., Marsik, F.J., Dvonch, J.T., 2015. Coupling atmospheric mercury isotope ratios and meteorology to identify sources of mercury impacting a coastal urban-industrial region near Pensacola, Florida, USA. Glob. Biogeochem. Cycles 29, 1689–1705. https://doi.org/10.1002/2015GB005146.
Domagalski, J., Majewski, M.S., Alpers, C.N., Eckley, C.S., Eagles-Smith, C.A., Schenk, L., Wherry, S., 2016. Comparison of mercury mass loading in streams to atmospheric deposition in watersheds of Western North America: Evidence for non-atmospheric mercury sources. Sci. Total Environ. 568, 638–650. https://doi.org/10.1016/j.scitotenv.2016.02.112.
Donovan, P.M., Blum, J.D., Yee, D., Gehrke, G.E., Singer, M.B., 2013. An isotopic record of mercury in San Francisco Bay sediment. Chem. Geol. 349, 87–98. https://doi.org/10.1016/j.chemgeo.2013.04.017.
Donovan, P.M., Blum, J.D., Demers, J.D., Gu, B., Brooks, S.C., Peryam, J., 2014. Identification of multiple mercury sources to stream sediments near Oak Ridge, TN, USA. Environ. Sci. Technol. 48, 3666–3674. https://doi.org/10.1021/es4046549.
Donovan, P.M., Blum, J.D., Singer, M.B., Marvin-DiPasquale, M., Tsui, M.T., 2016. Isotopic composition of inorganic mercury and methylmercury downstream of a historical gold mining region. Environ. Sci. Technol. 504, 1691–1702. https://doi.org/10.1021/acs.est.5b04413.
Douglas, T.A., Blum, J.D., 2019. Mercury isotopes reveal atmospheric gaseous mercury deposition directly to the arctic coastal snowpack. Environ. Sci. Technol. Lett. 6, 235–242. https://doi.org/10.1021/acs.estlett.9b00131.
Drevnick, P.E., Cooke, C.A., Barraza, D., Blais, J.M., Coale, K.H., Cumming, B.F., Curtis, C.J., Das, B., Donahue, W.F., Eagles-Smith, C.A., Engstrom, D.R., Fitzgerald, W.F., Furl, C.V., Gray, J.E., Hall, R.I., Jackson, T.A., Laird, K.R., Lockhart, W.L., Macdonald, R.W., Mast, M.A., Mathieu, C., Muir, D.C.G., Outridge, P.M., Reinemann, S.A., Rothenberg, S.E., Ruiz-Fernandez, S., Louis, V.L., Sanders, R.D., Sanei, H., Skierszkan, E.K., Van Metre, P.C., Veverica, T.J., Wiklund, J.A., Wolfe, B.B., 2016. Spatiotemporal patterns of mercury accumulation in lake sediments of western North America. Sci. Total Environ. 568, 1157–1170. https://doi.org/10.1016/j.scitotenv.2016.03.167.
Du, B., Feng, X., Li, P., Yin, R., Yu, B., Sonke, J.E., Guinot, B., Anderson, C.W.N., Maurice, L., 2018. Use of mercury isotopes to quantify mercury exposure sources in inland populations, China. Environ. Sci. Technol. 52 (9), 5407–5416. https://doi.org/10.1021/acs.est.7b05638.
Eagles-Smith, C.A., Ackerman, J.T., Willacker, J.J., Tate, M.T., Lutz, M.A., Fleck, J.A., Stewart, A.R., Wiener, J.G., Evers, D.C., Lepak, J.M., Davis, J.A., Pritz, C.F., 2016a. Spatial and temporal patterns of mercury concentrations in freshwater fish across the Western United States and Canada. Sci. Total Environ. 568, 1171–1184. https://doi.org/10.1016/j.scitotenv.2016.03.229.
Eagles-Smith, C.A., Wiener, J.G., Eckley, C.S., Willacker, J.J., Evers, D.C., Marvin-DiPasquale, M., Obrist, D., Fleck, J.A., Aiken, G.R., Lepak, J.M., Webster, J.P., Stewart, A.R., Davis, J.A., Alpers, C.N., Ackerman, J.T., 2016b. Mercury in western North America: a synthesis of environmental contamination, fluxes, bioaccumulation, and risk to fish and wildlife. Sci. Total Environ. 568, 1213–1226. https://doi.org/10.1016/j.scitotenv.2016.05.094.
Eckley, C.S., Hintelmann, H., 2006. Determination of mercury methylation potentials in the water column of lakes across Canada. Sci. Total Environ. 368 (1), 111–125. https://doi.org/10.1016/j.scitotenv.2005.09.042.
Enrico, M., Roux, G.L., Marusczak, N., Heimbürger, L.E., Claustres, A., Fu, X., Sun, R., Sonke, J.E., 2016. Atmospheric mercury transfer to peat bogs dominated by gaseous elemental mercury dry deposition. Environ. Sci. Technol. 50, 2405–2412. https://doi.org/10.1021/acs.est.5b06058.
Ericksen, J.A., Gustin, M.S., Schorran, D.E., Johnson, D.W., Lindberg, S.E., Coleman, J.S., 2003. Accumulation of atmospheric mercury in forest foliage. Atmos. Environ. 37 (12), 1613–1622. https://doi.org/10.1016/s1352-2310(03)00008-6.
Estrade, N., Carignan, J., Sonke, J.E., Donard, O.F., 2009. Mercury isotope fractionation during liquid–vapor evaporation experiments. Geochim. Cosmochim. Acta 73 (10), 2693–2711. https://doi.org/10.1016/j.gca.2009.01.024.
Estrade, N., Carignan, J., Donard, O.F., 2011. Tracing and quantifying anthropogenic mercury sources in soils of northern France using isotopic signatures. Environ. Sci. Technol. 45, 1235–1242. https://doi.org/10.1021/es1026823.
Feng, X., Foucher, D., Hintelmann, H., Yan, H., He, T., Qiu, G., 2010. Tracing mercury contamination sources in sediments using mercury isotope compositions. Environ. Sci. Technol. 44 (9), 3363–3368. https://doi.org/10.1021/es9039488.
Fleck, J.A., Marvin-DiPasquale, M., Eagles-Smith, C.A., Ackerman, J.T., Lutz, M.A., Tate, M., Alpers, C.N., Hall, B.D., Krabbenhoft, D.P., Eckley, C.S., 2016. Mercury and methylmercury in aquatic sediment across western North America. Sci. Total Environ. 568, 727–738. https://doi.org/10.1016/j.scitotenv.2016.03.044.
Foucher, D., Hintelmann, H., 2006. High-precision measurement of mercury isotope ratios in sediments using cold-vapor generation multi-collector inductively coupled plasma mass spectrometry. Anal. Bioanal. Chem. 384, 1470–1478. https://doi.org/10.1007/s00216-006-0373-x.
Foucher, D., Hintelmann, H., 2009. Tracing mercury contamination from the Idrija mining region (Slovenia) to the Gulf of Trieste using Hg isotope ratio measurements. Environ. Sci. Technol. 43 (1), 33–39. https://doi.org/10.1021/es801772b.
Foucher, D., Hintelmann, H., Al, T.A., MacQuarrie, K.T., 2013. Mercury isotope fractionation in waters and sediments of the Murray Brook mine watershed (New Brunswick, Canada): tracing mercury contamination and transformation. Chem. Geol. 336, 87–95. https://doi.org/10.1016/j.chemgeo.2012.04.014.
Friedli, H.R., Arellano, A.F., Cinnirella, S., Pirrone, N., 2009. Mercury emissions from global biomass burning: spatialand temporal distribution. In: Mercury Fate and Transport in the Global Atmosphere. Springer, Boston, MA, pp. 193–220. https://doi.org/10.1007/978-0-387-93958-2_8.
Fu, X., Marusczak, N., Wang, X., Gheusi, F., Sonke, J.E., 2016. Isotopic composition of gaseous elemental mercury in the free troposphere of the Pic du Midi Observatory, France. Environ. Sci. Technol. 50 (11), 5641–5650. https://doi.org/10.1021/acs.est.6b00033.
Gantner, N., Hintelmann, H., Zheng, W., Muir, D.C., 2009. Variations in stable isotope fractionation of Hg in food webs of Arctic lakes. Environ. Sci. Technol. 43 (24), 9148–9154. https://doi.org/10.1021/es901771r.
Gehrke, G.E., Blum, J.D., Meyers, P.A., 2009. The geochemical behavior and isotopic composition of Hg in a mid-Pleistocene western Mediterranean sapropel. Geochim. Cosmochim. Acta 73 (6), 1651–1665. https://doi.org/10.1016/j.gca.2008.12.012.
Gehrke, G.E., Blum, J.D., Marvin-DiPasquale, M., 2011a. Sources of mercury to San Francisco Bay surface sediment as revealed by mercury stable isotopes. Geochim. Cosmochim. Acta 75, 691–705. https://doi.org/10.1016/j.gca.2010.11.012.
Gehrke, G.E., Blum, J.D., Slotton, D.G., Greenfield, B.K., 2011b. Mercury isotopes link mercury in San Francisco Bay forage fish to surface sediments. Environ. Sci. Technol. 45, 1264–1270. https://doi.org/10.1021/es103053y.
Ghosh, S., Schauble, E.A., Couloume, G.L., Blum, J.D., Bergquist, B.A., 2013. Estimation of nuclear volume dependent fractionation of mercury isotopes in equilibrium liquid–vapor evaporation experiments. Chem. Geol. 336, 5–12. https://doi.org/10.1016/j.chemgeo.2012.01.008.
Gilmour, C.C., Henry, E.A., 1991. Mercury methylation in aquatic systems affected by acid deposition. Environ. Pollut. 71, 131–169. https://doi.org/10.1016/0269-7491(91)90031-q.
Gratz, L.E., Keeler, G.J., Blum, J.D., Sherman, L.S., 2010. Isotopic composition and fractionation of mercury in Great Lakes precipitation and ambient air. Environ. Sci. Technol. (20), 7764–7770. https://doi.org/10.1021/es100383w.
Gray, J.E., Pribil, M.J., Van Metre, P.C., Borrok, D.M., Thapalia, A., 2013. Identification of contamination in a lake sediment core using Hg and Pb isotopic compositions, Lake

Ballinger, Washington, USA. Appl. Geochem. 29, 1–12. https://doi.org/10.1016/j.apgeochem.2012.12.001.
Gray, J.E., Van Metre, P.C., Pribil, M.J., Horowitz, A.J., 2015. Tracing historical trends of Hg in the Mississippi River using Hg concentrations and Hg isotopic compositions in a lake sediment core, Lake Whittington, Mississippi, USA. Chem. Geol. 395, 80–87. https://doi.org/10.1016/j.chemgeo.2014.12.005.
Gustin, M.S., Evers, D.C., Bank, M.S., Hammerschmidt, C.R., Pierce, A., Basu, N., Blum, J.D., Bustamante, P., Chen, C., Driscoll, T.D., Horvat, M., Jaffe, D., Pacyna, J., Pirrone, N., Selin, N., 2016. Importance of integration and implementation of emerging and future mercury research into the Minamata Convention. Environ. Sci. Technol. 50 (6), 2767–2770. https://doi.org/10.1021/acs.est.6b00573.
Haitzer, M., Aiken, G.R., Ryan, J.N., 2002. Binding of mercury (II) to dissolved organic matter: the role of the mercury-to-DOM concentration ratio. Environ. Sci. Technol. 36 (16), 3564–3570. https://doi.org/10.1021/es025699i.
Hintelmann, H., Lu, S., 2003. High precision isotope ratio measurements of mercury isotopes in cinnabar ores using multi-collector inductively coupled plasma mass spectrometry. Analyst 128, 635–639. https://doi.org/10.1039/B300451A.
Huang, Q., Chen, J., Huang, W., Fu, P., Guinot, B., Feng, X.B., Shang, L.H., Wang, Z.H., Wang, Z.W., Yuan, S.L., Cai, H.M., Wei, L.F., B, Y., 2016. Isotopic composition for source identification of mercury in atmospheric fine particles. Atmos. Chem. Phys. Discuss. 16 (18), 11773–11786. https://doi.org/10.5194/acp-2016-363.
Huang, S., Sun, L., Zhou, T., Yuan, D., Du, B., Sun, X., 2018. Natural stable isotopic compositions of mercury in aerosols and wet precipitations around a coal-fired power plant in Xiamen, southeast China. Atmos. Environ. 173, 72–80. https://doi.org/10.1016/j.atmosenv.2017.11.003.
Janssen, S.E., Riva-Murray, K., DeWild, J.F., Ogorek, J.M., Tate, M.T., Van Metre, P.C., Krabbenhoft, D.P., Coles, J.F., 2019. Chemical and Physical Controls on Mercury Source Signatures in Stream Fish from the Northeastern United States. Environmental Science and Technology 53 (17), 10110–10119. https://doi.org/10.1021/acs.est.9b03394.
Janssen, S.E., Schaefer, J.K., Barkay, T., Reinfelder, J.R., 2016. Fractionation of mercury stable isotopes during microbial methylmercury production by iron-and sulfate-reducing bacteria. Environ. Sci. Technol. 50 (15), 8077–8083. https://doi.org/10.1021/acs.est.6b00854.
Jiménez-Moreno, M., Perrot, V., Epov, V.N., Monperrus, M., Amouroux, D., 2013. Chemical kinetic isotope fractionation of mercury during abiotic methylation of Hg (II) by methylcobalamin in aqueous chloride media. Chem. Geol. 336, 26–36. https://doi.org/10.1016/j.chemgeo.2012.08.029.
Jiménez-Moreno, M., Barre, J.P., Perrot, V., Bérail, S., Martín-Doimeadios, R.C.R., Amouroux, D., 2016. Sources and fate of mercury pollution in Almadén mining district (Spain): evidences from mercury isotopic compositions in sediments and lichens. Chemosphere 147, 430–438. https://doi.org/10.1016/j.chemosphere.2015.12.094.
Jiskra, M., Wiederhold, J.G., Bourdon, B., Kretzschmar, R., 2012. Solution speciation controls mercury isotope fractionation of Hg (II) sorption to goethite. Environ. Sci. Technol. 46 (12), 6654–6662. https://doi.org/10.1021/es3008112.
Jiskra, M., Wiederhold, J.G., Skyllberg, U., Kronberg, R.-M., Hajdas, I., Kretzschmar, R., 2015. Mercury deposition and re-emission pathways in boreal forest soils investigated with Hg isotope signatures. Environ. Sci. Technol. 49 (12), 7188–7196. https://doi.org/10.1021/acs.est.5b00742.
Jiskra, M., Wiederhold, J.G., Skyllberg, U., Kronberg, R.M., Kretzschmar, R., 2017. Source tracing of natural organic matter bound mercury in boreal forest runoff with mercury stable isotopes. Environ Sci Process Impacts 19 (10), 1235–1248. https://doi.org/10.1039/c7em00245a.
Jiskra, M., Marusczak, N., Leung, K.H., Hawkins, L., Prestbo, E., Sonke, J.E., 2019. Automated stable isotope sampling of gaseous elemental mercury (ISO-GEM): insights into GEM emissions from building surfaces. Environ. Sci. Technol. 53, 4346–4354. https://doi.org/10.1021/acs.est.8b06381.
Koster van Groos, P.G., Esser, B.K., Williams, R.W., Hunt, J.R., 2013. Isotope effect of mercury diffusion in air. Environ. Sci. Technol. 48 (1), 227–233. https://doi.org/10.1021/es4033666.
Kritee, K., Barkay, T., Blum, J.D., 2009. Mass dependent stable isotope fractionation of mercury during mer mediated microbial degradation of monomethylmercury. Geochim. Cosmochim. Acta 73 (5), 1285–1296. https://doi.org/10.1016/j.gca.2008.11.038.
Kumar, A., Wu, S., Huang, Y., Liao, H., Kaplan, J.O., 2018. Mercury from wildfires: global emission inventories and sensitivity to 2000–2050 global change. Atmos. Environ. 173, 6–15. https://doi.org/10.1016/j.atmosenv.2017.10.061.
Kwon, S.Y., Selin, N.E., 2016. Uncertainties in atmospheric mercury modeling for policy evaluation. Curr. Pollut. Rep. 2, 103–114. https://doi.org/10.1007/s40726-016-0030-8.
Kwon, S.Y., Blum, J.D., Carvan, M.J., Basu, N., Head, J.A., Madenjian, C.P., David, S.R., 2012. Absence of fractionation of mercury isotopes during trophic transfer of methylmercury to freshwater fish in captivity. Environ. Sci. Technol. 46, 7527–7534. https://doi.org/10.1021/es300794q.
Kwon, S.Y., Blum, J.D., Chirby, M.A., Chesney, E.J., 2013. Application of mercury isotopes for tracing trophic transfer and internal distribution of mercury in marine fish feeding experiments. Environ. Toxicol. Chem. 32, 2322–2330. https://doi.org/10.1002/etc.2313.
Kwon, S.Y., Blum, J.D., Chen, C.Y., Meattey, D.E., Mason, R.P., 2014. Mercury isotope study of sources and exposure pathways of methylmercury in estuarine food webs in the Northeastern US. Environ. Sci. Technol. 48, 10089–10097. https://doi.org/10.1021/es5020554.
Kwon, S.Y., Blum, J.D., Nadelhoffer, K.J., Dvonch, J.T., Tsui, M.T.K., 2015. Isotopic study of mercury sources and transfer between a freshwater lake and adjacent forest food web. Sci. Total Environ. 532, 220–229. https://doi.org/10.1016/j.scitotenv.2015.06.012.
Kwon, S.Y., Blum, J.D., Madigan, D.J., Block, B.A., Popp, B.N., 2016. Quantifying mercury isotope dynamics in captive Pacific bluefin tuna (Thunnus orientalis). Elem. Sci. Anth. 4. https://doi.org/10.12952/journal.elementa.000088.
Kwon, S.Y., Selin, N.E., Giang, A., Karplus, V.J., Zhang, D., 2018. Present and future mercury concentrations in Chinese rice: insights from modeling. Global Biogeochem. Cyc. 32, 437–462. https://doi.org/10.1002/2017GB005824.
Laffont, L., Sonke, J.E., Maurice, L., Monrroy, S.L., Chincheros, J., Amouroux, D., Behra, P., 2011. Hg speciation and stable isotope signatures in human hair as a tracer for dietary and occupational exposure to mercury. Environ. Sci. Technol. 45, 9910–9916. https://doi.org/10.1021/es202353m.
Lepak, R.F., Yin, R., Krabbenhoft, D.P., Ogorek, J.M., DeWild, J.F., Holsen, T.M., Hurley, J.P., 2015. Use of stable isotope signatures to determine mercury sources in the Great Lakes. Environ. Sci. Technol. Lett. 2, 335–341. https://doi.org/10.1021/acs.estlett.5b00277.
Lepak, R.F., Janssen, S.E., Yin, R., Krabbenhoft, D.P., Ogorek, J.M., DeWild, J.F., Tate, M.T., Holsen, T.M., Hurley, J.P., 2018. Factors affecting mercury stable isotopic distribution in piscivorous fish of the Laurentian Great Lakes. Environ. Sci. Technol. 52, 2768–2776. https://doi.org/10.1021/acs.est.7b06120.
Li, P., Feng, X.B., Qiu, G.L., Shang, L.H., Li, Z.G., 2009. Mercury pollution in Asia: a review of the contaminated sites. J. Hazard. Mater. 168 (2), 591–601. https://doi.org/10.1016/j.jhazmat.2009.03.031.
Li, M., Sherman, L.S., Blum, J.D., Grandjean, P., Mikkelsen, B., Weihe, P., Sunderland, E.M., Shine, J.P., 2014. Assessing sources of human methylmercury exposure using stable mercury isotopes. Environ. Sci. Technol. 48 (15), 8800–8806. https://doi.org/10.1021/es500340r.
Li, M., Schartup, A.T., Valberg, A.P., Ewald, J.D., Krabbenhoft, D.P., Yin, R., Balcom, P.H., Sunderland, E.M., 2016. Environmental origins of methylmercury accumulated in subarctic estuarine fish indicated by mercury stable isotopes. Environ. Sci. Technol. 50 (21), 11559–11568. https://doi.org/10.1021/acs.est.6b03206.
Liu, J., Feng, X.B., Yin, R.S., Zhu, W., Li, Z., 2011. Mercury distributions and mercury isotope signatures in sediments of Dongjiang River, the Pearl River Delta. China. Chem. Geol. 287, 81–89. https://doi.org/10.1016/j.chemgeo.2011.06.001.
Liu, C.B., Hua, X.B., Liu, H.W., Yu, B., Mao, Y.X., Wang, D.Y., Yin, Y.G., Hu, L., Shi, J.B., Jiang, G.B., 2018. Tracing aquatic bioavailable Hg in three different regions of China using fish Hg isotopes. Ecotox. Environ. Safe. 150, 327–334. https://doi.org/10.1016/j.ecoenv.2017.12.053.
Loseto, L.L., Siciliano, S.D., Lean, D.R., 2004. Methylmercury production in High Arctic wetlands. Environ. Toxicol. Chem. 23 (1), 17–23. https://doi.org/10.1897/02-644.
Ma, J., Hintelmann, H., Kirk, J.L., Muir, D.C., 2013. Mercury concentrations and mercury isotope composition in lake sediment cores from the vicinity of a metal smelting facility in Flin Flon, Manitoba. Chem. Geol. 336, 96–102. https://doi.org/10.1016/j.chemgeo.2012.10.037.
Madigan, D.J., Li, M., Yin, R., Baumann, H., Snodgrass, O.E., Dewar, H., Krabbenhoft, D.P., Baumann, Z., Fisher, N.S., Balcom, P., Sunderland, E.M., 2018. Mercury stable isotopes reveal influence of foraging depth on mercury concentrations and growth in Pacific bluefin tuna. Environ. Sci. Technol. 52, 6256–6264. https://doi.org/10.1021/acs.est.7b06429.
Mao, H., Ye, Z., Driscoll, C., 2017. Meteorological effects on Hg wet deposition in a forested site in the Adirondack region of New York during 2000–2015. Atmos. Environ. 168, 90–100. https://doi.org/10.1016/j.atmosenv.2017.08.058.
Masbou, J., Point, D., Sonke, J.E., Frappart, F., Perrot, V., Amouroux, D., Richard, P., Becker, P.R., 2015. Hg stable isotope time trend in ringed seals registers decreasing sea ice cover in the Alaskan Arctic. Environ. Sci. Technol. 49 (15), 8977–8985. https://doi.org/10.1021/es5048446.
Masbou, J., Sonke, J.E., Amouroux, D., Guillou, G., Becker, P.R., Point, D., 2018. Hg-Stable isotope variations in marine top predators of the western Arctic ocean. Earth Space Chem. 2, 479–490. https://doi.org/10.1021/acsearthspacechem.8b00017.
Mead, C., Lyons, J.R., Johnson, T.M., Anbar, A.D., 2013. Unique Hg stable isotope signatures of compact fluorescent lamp-sourced Hg. Environ. Sci. Technol. 47 (6), 2542–2547. https://doi.org/10.1021/es303940p.
Meng, M., Sun, R.Y., Liu, H.W., Yu, B., Yin, Y.G., Hu, L.G., Shi, J.B., Jiang, G.B., 2019. An integrated model for input and migration of mercury in Chinese coastal sediments. Environ. Sci. Technol. 53, 2460–2471. https://doi.org/10.1021/acs.est.8b06329.
Mergler, D., Anderson, H.A., Chan, L.H.M., Mahaffey, K.R., Murray, M., Sakamoto, M., Stern, A.H., 2007. Methylmercury exposure and health effects in humans: a worldwide concern. AMBIO: J. Hum. Environ. 36 (1), 3–11. https://doi.org/10.1579/0044-7447(2007)36[3:meahei]2.0.co;2.
Mil-Homens, M., Blum, J., Canário, J., Caetano, M., Costa, A.M., Lebreiro, S.M., Trancoso, M., Richter, T., de Stigter, H., Johnson, M., Branco, V., Cesario, R., Mouro, F., Mateus, M., Boer, W., Melo, Z., 2013. Tracing anthropogenic Hg and Pb input using stable Hg and Pb isotope ratios in sediments of the central Portuguese Margin. Chem. Geol. 336, 62–71. https://doi.org/10.1016/j.chemgeo.2012.02.018.
Montzka, S.A., Reimann, S., Engel, A., Kruger, K., Doherty, K., Sturges, W.T., Blake, D., Dorf, M., Fraser, P., Froidevaux, L., Jucks, K., Kreher, K., Kurylo, M.J., Mellouki, A., Miller, J., Nielsen, O.-J., Orkin, V.L., Prinn, R.G., Rhew, R., Santee, M.L., Stohl, A., Verdonik, D., 2011. Ozone Depleting Substances (ODSs) and Related Chemicals. World Meteorological Organization.
Motta, L.C., Blum, J.D., Johnson, M.W., Umhau, B.P., Popp, B.N., Washburn, S.J., Drazen, J.C., Benitez-Nelson, C.R., Hannides, C.C.S., Close, H.G., Lamborg, C.H., 2019. Mercury cycling in the North Pacific Subtropical Gyre as revealed by mercury stable isotope ratios. Global Biogeochem. Cyc. 33, 777–794. https://doi.org/10.1029/2018GB006057.
Obrist, D., Pokharel, A.K., Moore, C., 2014. Vertical profile measurements of soil air suggest immobilization of gaseous elemental mercury in mineral soil. Environ. Sci. Technol. 48, 2242–2252. https://doi.org/10.1021/es4048297.
Obrist, D., Kirk, J.L., Zhang, L., Sunderland, E.M., Jiskra, M., Selin, N.E., 2018. A review

of global environmental mercury processes in response to human and natural perturbations: changes of emissions, climate, and land use. Ambio 47 (2), 116–140. https://doi.org/10.1007/s13280-017-1004-9.
Pacyna, J.M., Pacyna, E.G., Steenhuisen, F., Wilson, S., 2003. Mapping 1995 global anthropogenic emissions of mercury. Atmos. Environ. 37, 109–117. https://doi.org/10.1016/s1352-2310(03)00239-5.
Pérez-Rodríguez, M., Biester, H., Aboal, J.R., Toro, M., Cortizas, A.M., 2019. Thawing of snow and ice caused extraordinary high and fast mercury fluxes to lake sediments in Antarctica. Geochim. Cosmochim. Acta 248, 109–122. https://doi.org/10.1016/j.gca.2019.01.009.
Perlinger, J.A., Urban, N.R., Giang, A., Selin, N.E., Hendricks, A.N., Zhang, H., Kumar, A., Wu, S., Gagnon, V.S., Norman, E.S., 2018. Responses of deposition and bioaccumulation in the Great Lakes region to policy and other large-scale drivers of mercury emissions. Environ Sci Process Impacts 20 (1), 195–209. https://doi.org/10.1039/c7em00547d.
Perrot, V., Epov, V.N., Pastukhov, M.V., Grebenshchikova, V.I., Zouiten, C., Sonke, J.E., Husted, S., Donard, O.F.X., Amouroux, D., 2010. Tracing sources and bioaccumulation of mercury in fish of Lake Baikal − Angara River using Hg isotopic composition. Environ. Sci. Technol. 44, 8030–8037. https://doi.org/10.1021/es101898e.
Perrot, V., Pastukhov, M.V., Epov, V.N., Husted, S., Donard, O.F., Amouroux, D., 2012. Higher mass-independent isotope fractionation of methylmercury in the pelagic food web of Lake Baikal (Russia). Environ. Sci. Technol. 46, 5902–5911. https://doi.org/10.1021/es204572g.
Perrot, V., Bridou, R., Pedrero, Z., Guyoneaud, R., Monperrus, M., Amouroux, D., 2015. Identical Hg isotope mass dependent fractionation signature during methylation by sulfate-reducing bacteria in sulfate and sulfate-free environment. Environ. Sci. Technol. 49 (3), 1365–1373. https://doi.org/10.1021/es5033376.
Perrot, V., Masbou, J., Pastukhov, M.V., Epov, V.N., Point, D., Bérail, S., Becker, P.R., Sonke, J.E., Amouroux, D., 2016. Natural Hg isotopic composition of different Hg compounds in mammal tissues as a proxy for in vivo breakdown of toxic methylmercury. Metallomics 8 (2), 170–178. https://doi.org/10.1039/c5mt00286a.
Ravichandran, M., 2004. Interactions between mercury and dissolved organic matter—a review. Chemosphere 55, 319–331. https://doi.org/10.1016/j.chemosphere.2003.11.011.
Rea, A.W., Lindberg, S.E., Keeler, G.J., 2000. Assessment of dry deposition and foliar leaching of mercury and selected trace elements based on washed foliar and surrogate surfaces. Environ. Sci. Technol. 34 (12), 2418–2425. https://doi.org/10.1021/es991305k.
Rea, A.W., Lindberg, S.E., Scherbatskoy, T., Keeler, G.J., 2002. Mercury accumulation in foliage over time in two northern mixedhardwood forests. Water Air Soil Pollut. 133 (1–4), 49–67. https://doi.org/10.1023/A:1012919731598.
Rodriguez-Gonzalez, P., Epov, V.N., Bridou, R., Tessier, E., Guyoneaud, R., Monperrus, M., Amouroux, D., 2009. Species-specfic stable isotope fractionation of mercury during Hg(II) methylation by anaerobic bacteria (Desulfobulbus propionicus) under dark conditions. Environ. Sci. Technol. 43 (24), 9183–9188. https://doi.org/10.1021/es902206j.
Rolison, J.M., Landing, W.M., Luke, W., Cohen, M., Salters, V.J.M., 2013. Isotopic composition of species-specific atmospheric Hg in a coastal environment. Chem. Geol. 336, 37–49. https://doi.org/10.1016/j.chemgeo.2012.10.007.
Rua-Ibarz, A., Bolea-Fernandez, E., Maage, A., Frantzen, S., Valdersnes, S., Vanhaecke, F., 2016. Assessment of Hg pollution released from a WWII Submarine Wreck (U-864) by Hg isotopic analysis of sediments and cancer pagurus tissues. Environ. Sci. Technol. 50 (19), 10361–10369. https://doi.org/10.1021/acs.est.6b02128.
Sackett, D.K., Drazen, J.C., Choy, C.A., Popp, B., Pitz, G.L., 2015. Mercury sources and trophic ecology for Hawaiian bottomfish. Environ. Sci. Technol. 49, 6909–6918. https://doi.org/10.1021/acs.est.5b01009.
Schauble, E.A., 2007. Role of nuclear volume in driving equilibrium stable isotope fractionation of mercury, thallium, and other very heavy elements. Geochim. Cosmochim. Acta 71 (9), 2170–2189. https://doi.org/10.1016/j.gca.2007.02.004.
Schroeder, W.H., Munthe, J., 1998. Atmospheric mercury—an overview. Atmos. Environ. 32 (5), 809–822. https://doi.org/10.1016/s1352-2310(97)00293-8.
Schudel, G., Miserendino, R.A., Veiga, M.M., Velasquez-López, P.C., Lees, P.S., Winland-Gaetz, S., Guimarães, J.R.D., Bergquist, B.A., 2018. An investigation of mercury sources in the Puyango-Tumbes River: Using stable Hg isotopes to characterize transboundary Hg pollution. Chemosphere 202, 777–787. https://doi.org/10.1016/j.chemosphere.2018.03.081.
Selin, N.E., 2009. Global biogeochemical cycling of mercury: a review. Annu. Rev. Environ. Resour. 34 (1), 43–63. https://doi.org/10.1146/annurev.environ.051308.084314.
Senn, D.B., Chesney, E.J., Blum, J.D., Bank, M.S., Maage, A., Shine, J.P., 2010. Stable isotope (N, C, Hg) study of methylmercury sources and trophic transfer in the northern Gulf of Mexico. Environ. Sci. Technol. 44, 1630–1637. https://doi.org/10.1021/es902361j.
Sherman, L.S., Blum, J.D., 2013. Mercury stable isotopes in sediments and largemouth bass from Florida lakes, USA. Sci. Total Environ. 448, 163–175. https://doi.org/10.1016/j.scitotenv.2012.09.038.
Sherman, L.S., Blum, J.D., Johnson, K.P., Keeler, G.J., Barres, J.A., Douglas, T.A., 2010. Mass-independent fractionation of mercury isotopes in Arctic snow driven by sunlight. Nat. Geosci. 3, 173. https://doi.org/10.1038/ngeo758.
Sherman, L.S., Blum, J.D., Keeler, G.J., Demers, J.D., Dvonch, J.T., 2012. Investigation of local mercury deposition from a coal-fired power plant using mercury isotopes. Environ. Sci. Technol. 46 (1), 382–390. https://doi.org/10.1021/es202793c.
Sherman, L.S., Blum, J.D., Basu, N., Rajaee, M., Evers, D.C., Buck, D.G., Petrlik, J., DiGangi, J., 2015a. Assessment of mercury exposure among small-scale gold miners using mercury stable isotopes. Environ. Res. 137, 226–234. https://doi.org/10.1016/j.envres.2014.12.021.
Sherman, L.S., Blum, J.D., Dvonch, J.T., Gratz, L.E., Landis, M.S., 2015b. The use of Pb, Sr, and Hg isotopes in Great Lakes precipitation as a tool for pollution source attribution. Sci. Total Environ. 502, 362–374. https://doi.org/10.1016/j.scitotenv.2014.09.034.
Slemr, F., Brunke, E.G., Ebinghaus, R., Kuss, J., 2011. Worldwide trend of atmospheric mercury since 1995. Atmos. Chem. Phys. 11 (10), 4779–4787. https://doi.org/10.5194/acp-11-4779-2011.
Smith, C.N., Kesler, S.E., Blum, J.D., Rytuba, J.J., 2008. Isotope geochemistry of mercury in source rocks, mineral deposits and spring deposits of the California coast ranges, USA. Earth Planet. Sci. Lett. 269 (3–4), 399–407. https://doi.org/10.1016/j.epsl.2008.02.029.
Smith, R.S., Wiederhold, J.G., Jew, A.D., Brown Jr., G.E., Bourdon, B., Kretzschmar, R., 2014. Small-scale studies of roasted ore waste reveal extreme ranges of stable mercury isotope signatures. Geochim. Cosmochim. Acta 137, 1–17. https://doi.org/10.1016/j.gca.2014.03.037.
Smith, R.S., Wiederhold, J.G., Kretzschmar, R., 2015. Mercury isotope fractionation during precipitation of metacinnabar (β-HgS) and montroydite (HgO). Environ. Sci. Technol. 49 (7), 4325–4334. https://doi.org/10.1021/acs.est.5b00409.
Soerensen, A.L., Jacob, D.J., Streets, D.G., Witt, M.L., Ebinghaus, R., Mason, R.P., Andersson, M., Sunderland, E.M., 2012. Multi-decadal decline of mercury in the North Atlantic atmosphere explained by changing subsurface seawater concentrations. Geophys. Res. Lett. 39 (21). https://doi.org/10.1029/2012gl053736.
Sonke, J.E., 2011. A global model of mass independent mercury stable isotope fractionation. Geochim. Cosmochim. Acta 75, 4577–4590. https://doi.org/10.1016/j.gca.2011.05.027.
Sonke, J.E., Schäfer, J., Chmeleff, J., Audry, S., Blanc, G., Dupré, B., 2010. Sedimentary mercury stable isotope records of atmospheric and riverine pollution from two major European heavy metal refineries. Chem. Geol. 279, 90–100. https://doi.org/10.1016/j.chemgeo.2010.09.017.
Sprovieri, F., Pirrone, N., Bencardino, M., D'Amore, F., Angot, H., Barbante, C., Brunke, E.G., Arcega-Cabrera, F., Cairns, W., Comero, S., Diéguez, M.D.C., 2017. Five-year records of mercury wet deposition flux at GMOS sites in the Northern and Southern hemispheres. Atmos. Chem. Phys. 17 (4), 2689–2708. https://doi.org/10.5194/acp-17-2689-2017.
Sun, R., Heimbürger, L.E., Sonke, J.E., Liu, G., Amouroux, D., Berail, S., 2013. Mercury stable isotope fractionation in six utility boilers of two large coal-fired power plants. Chem. Geol. 336, 103–111. https://doi.org/10.1016/j.chemgeo.2012.10.055.
Sun, R., Sonke, J.E., Heimbürger, L.E., Belkin, H.E., Liu, G., Shome, D., Cukrowska, E., Liousse, C., Pokrovsky, O.S., Streets, D.G., 2014. Mercury stable isotope signatures of world coal deposits and historical coal combustion emissions. Environ. Sci. Technol. 48, 7660–7668. https://doi.org/10.1021/es501208a.
Sun, G., Sommar, J., Feng, X., Lin, C.J., Ge, M., Wang, W., Yin, R., Fu, X., Shang, L., 2016a. Mass-dependent and-independent fractionation of mercury isotope during gas-phase oxidation of elemental mercury vapor by atomic Cl and Br. Environ. Sci. Technol. 50 (17), 9232–9241. https://doi.org/10.1021/acs.est.6b01668.
Sun, R., Sonke, J.E., Liu, G., 2016b. Biogeochemical controls on mercury stable isotope compositions of world coal deposits: A review. Earth Sci. Rev. 152, 1–13. https://doi.org/10.1016/j.earscirev.2015.11.005.
Sun, R., Streets, D.G., Horowitz, H.M., Amos, H.M., Liu, G., Perrot, V., Toutain, J.P., Hintelmann, H., Sunderland, E.M., Sonke, J.E., 2016c. Historical (1850–2010) mercury stable isotope inventory from anthropogenic sources to the atmosphere. Elem Sci Anth 4, 1–15. https://doi.org/10.12952/journal.elementa.000091.
Sun, R., Jiskra, M., Amos, H.M., Zhang, Y., Sunderland, E.M., Sonke, J.E., 2019. Modelling the mercury stable isotope distribution of Earth surface reservoirs: Implications for global Hg cycling. Geochim. Cosmochim. Acta 246, 156–173. https://doi.org/10.1016/j.gca.2018.11.036.
Sunderland, E.M., Krabbenhoft, D.P., Moreau, J.W., Strode, S.A., Landing, W.M., 2009. Mercury sources, distribution, and bioavailability in the North Pacific Ocean: Insights from data and models. Global Biogeochem. Cyc. 23, 1–14. https://doi.org/10.1029/2008GB003425.
Tsui, M.T.K., Blum, J.D., Kwon, S.Y., Finlay, J.C., Balogh, S.J., Nollet, Y.H., 2012. Sources and transfers of methylmercury in adjacent river and forest food webs. Environ. Sci. Technol. 46, 10957–10964. https://doi.org/10.1021/es3019836.
Tsui, M.T.K., Blum, J.D., Finlay, J.C., Balogh, S.J., Nollet, Y.H., Palen, W.J., Power, M.E., 2014. Variation in terrestrial and aquatic sources of methylmercury in stream predators as revealed by stable mercury isotopes. Environ. Sci. Technol. 48 (17), 10128–10135. https://doi.org/10.1021/es500517s.
Tsui, M.T.K., Adams, E.M., Jackson, A.K., Evers, D.C., Blum, J.D., Balogh, S.J., 2018. Understanding sources of methylmercury in songbirds with stable mercury isotopes: Challenges and future directions. Environ. Toxicol. Chem. 37 (1), 166–174. https://doi.org/10.1002/etc.3941.
Ullrich, S.M., Tanton, T.W., Abdrashitova, S.A., 2001. Mercury in the aquatic environment: A review of factors affecting methylation. Crit. Rev. Environ. Sci. Technol. 31 (3), 241–293. https://doi.org/10.1080/20016491089226.
United Nations Environment (UN Environment), 2017a. Minamata Convention on Mercury—Text and Annexes. http://www.mercuryconvention.org/Portals/11/documents/Booklets/COP1%20version/Minamata-Convention-booklet-eng-full.pdf (accessed 15 August 2019).
United Nations Environment (UN Environment), 2017b. Stockholm Convention on Persistent Organic Pollutions (POPs)—Text and Annexes. http://www.pops.int/TheConvention/Overview/TextoftheConvention/tabid/2232/Default.aspx (accessed 15 August 2019).
Wang, X., Luo, J., Yin, R., Yuan, W., Lin, C.J., Sommar, J., Feng, X., Wang, H., Lin, C., 2016. Using mercury isotopes to understand mercury accumulation in the montane forest floor of the Eastern Tibetan Plateau. Environ. Sci. Technol. 51 (2), 801–809. https://doi.org/10.1021/acs.est.6b03806.

Washburn, S.J., Blum, J.D., Demers, J.D., Kurz, A.Y., Landis, R.C., 2017. Isotopic characterization of mercury downstream of historic industrial contamination in the South River, Virginia. Environ. Sci. Technol. 51, 10965–10973. https://doi.org/10.1021/acs.est.7b02577.

Weiss-Penzias, P.S., Gay, D.A., Brigham, M.E., Parsons, M.T., Gustin, M.S., ter Schure, A., 2016. Trends in mercury wet deposition and mercury air concentrations across the US and Canada. Sci. Total Environ. 568, 546–556. https://doi.org/10.1016/j.scitotenv.2016.01.061.

Wiederhold, J.G., Cramer, C.J., Daniel, K., Infante, I., Bourdon, B., Kretzschmar, R., 2010. Equilibrium mercury isotope fractionation between dissolved Hg(II) species and thiol-bound Hg. Environ. Sci. Technol. 44 (11), 4191–4197. https://doi.org/10.1021/es100205t.

Wiederhold, J.G., Smith, R.S., Siebner, H., Jew, A.D., Brown Jr., G.E., Bourdon, B., Kretzschmar, R., 2013. Mercury isotope signatures as tracers for Hg cycling at the New Idria Hg mine. Environ. Sci. Technol. 47, 6137–6145. https://doi.org/10.1021/es305245z.

Wiederhold, J.G., Skyllberg, U., Drott, A., Jiskra, M., Jonsson, S., Bjorn, E., Bourdon, B., Kretzschmar, R., 2015. Mercury isotope signatures in contaminated sediments as a tracer for local industrial pollution sources. Environ. Sci. Technol. 49 (1), 177–185. https://doi.org/10.1021/es5044358.

Woerndle, G.E., Tsui, M.T., Sebestyen, S.D., Blum, J.D., Nie, X., Kolka, R.K., 2018. New insights on ecosystem mercury cycling revealed by stable isotopes of mercury in water flowing from a headwater peatland catchment. Environ. Sci. Technol. 52 (4), 1854–1861. https://doi.org/10.1021/acs.est.7b04449.

World Health Organization, 2018. Ten Chemicals of Major Public Health Concern. http://www.who.int/ipcs/assessment/public_health/chemicals_phc/en/ (accessed 15 August 2019).

Xu, H., Sonke, J.E., Guinot, B., Fu, X., Sun, R., Lanzanova, A., Candaudap, F., Shen, Z., Cao, J., 2017. Seasonal and annual variations in atmospheric Hg and Pb isotopes in Xi'an, China. Environ. Sci. Technol. 51 (7), 3759–3766. https://doi.org/10.1021/acs.est.6b06145.

Yin, R., Feng, X., Meng, B., 2013a. Stable mercury isotope variation in rice plants (Oryza sativa L.) from the Wanshan mercury mining district, SW China. Environ. Sci. Technol. 47 (5), 2238–2245. https://doi.org/10.1021/es304302a.

Yin, R., Feng, X., Wang, J., Bao, Z., Yu, B., Chen, J., 2013b. Mercury isotope variations between bioavailable mercury fractions and total mercury in mercury contaminated soil in Wanshan Mercury Mine, SW China. Chem. Geol. 336, 80–86. https://doi.org/10.1016/j.chemgeo.2012.04.017.

Yin, R., Feng, X., Wang, J., Li, P., Liu, J., Zhang, Y., Chen, J., Zheng, L., Hu, T., 2013c. Mercury speciation and mercury isotope fractionation during ore roasting process and their implication to source identification of downstream sediment in the Wanshan mercury mining area, SW China. Chem. Geol. 336, 72–79. https://doi.org/10.1016/j.chemgeo.2012.04.030.

Yin, R., Feng, X., Li, X., Yu, B., Du, B., 2014. Trends and advances in mercury stable isotopes as a geochemical tracer. Trends Environ. Anal. Chem. 2, 1–10. https://doi.org/10.1016/j.teac.2014.03.001.

Yin, R., Feng, X., Chen, B., Zhang, J., Wang, W., Li, X., 2015. Identifying the sources and processes of mercury in subtropical estuarine and ocean sediments using Hg isotopic composition. Environ. Sci. Technol. 49 (3), 1347–1355. https://doi.org/10.1021/es504070y.

Yin, R., Feng, X., Zhang, J., Pan, K., Wang, W., Li, X., 2016. Using mercury isotopes to understand the bioaccumulation of Hg in the subtropical Pearl River Estuary, South China. Chemosphere 147, 173–179. https://doi.org/10.1016/j.chemosphere.2015.12.100.

Yu, B., Fu, X., Yin, R., Zhang, H., Wang, X., Lin, C.J., Wu, C., Zhang, Y., He, N., Fu, P., Wang, Z., Shang, L., Sommar, J., Sonke, J.E., Maurice, L., Guinot, B., Feng, X., 2016. Isotopic composition of atmospheric mercury in China: new evidence for sources and transformation processes in air and in vegetation. Environ. Sci. Technol. 50 (17), 9262–9269. https://doi.org/10.1021/acs.est.6b01782.

Yuan, S., Zhang, Y., Chen, J., Kang, S., Zhang, J., Feng, X., Cai, H., Wang, Z., Wang, Z., Huang, Q., 2015. Large variation of mercury isotope composition during a single precipitation event at Lhasa City, Tibetan Plateau, China. Proced. Earth Plan. Sci. 13, 282–286. https://doi.org/10.1016/j.proeps.2015.07.066.

Yuan, W., Sommar, J., Lin, C.J., Wang, X., Li, K., Liu, Y., Zhang, H., Lu, Z., Wu, C., Feng, X., 2019. Stable isotope evidence shows re-emission of elemental mercury vapor occurring after reductive loss from foliage. Environ. Sci. Technol. 53 (2), 651–660. https://doi.org/10.1021/acs.est.8b04865.

Zhang, Y., Jacob, D.J., Horowitz, H.M., Chen, L., Amos, H.M., Krabbenhoft, D.P., Slemr, F., St. Louis, V.L., Sunderland, E.M., 2016. Observed decrease in atmospheric mercury explained by global decline in anthropogenic emissions. Proc. Natl. Acad. Sci. 113 (3), 526–531. https://doi.org/10.1073/pnas.1516312113.

Zheng, W., Foucher, D., Hintelmann, H., 2007. Mercury isotope fractionation during volatilization of Hg(0) from solution into the gas phase. Journal of Analytical Atomic Spectrometry 22, 1097–1104. https://doi.org/10.1039/b705677j.

Zheng, W., Hintelmann, H., 2009. Mercury isotope fractionation during photoreduction in natural water is controlled by its Hg/DOC ratio. Geochim. Cosmochim. Acta 73, 6704–6715. https://doi.org/10.1016/j.gca.2009.08.016.

Zheng, W., Hintelmann, H., 2010a. Isotope fractionation of mercury during its photochemical reduction by low-molecular-weight organic compounds. J. Phys. Chem. A 114 (12), 4246–4253. https://doi.org/10.1021/jp9111348.

Zheng, W., Hintelmann, H., 2010b. Nuclear field shift effect in isotope fractionation of mercury during abiotic reduction in the absence of light. J. Phys. Chem. A 114 (12), 4238–4245. https://doi.org/10.1021/jp910353y.

Zheng, W., Obrist, D., Weis, D., Bergquist, B.A., 2016. Mercury isotope compositions across North American forests. Glob. Biogeochem. Cycles 30 (10), 1475–1492. https://doi.org/10.1002/2015gb005323.

Zheng, W., Demers, J.D., Lu, X., Bergquist, B.A., Anbar, A.D., Blum, J.D., Gu, B., 2019. Mercury stable isotope fractionation during abiotic dark oxidation in the presence of thiols and natural organic matter. Environ. Sci. Technol. 53 (4), 1853–1862. https://doi.org/10.1021/acs.est.8b05047.